Journal Pre-proof

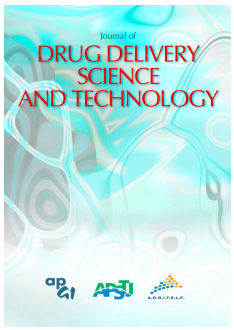

Development of pimozide spray dried lipid nanoparticles with enhanced targeting of non-small cell lung cancer

Arwa Omar Al Khatib, Amal Yousfan, Anas Abed, Mohamed El-Tanani, Hisham Al-Obaidi

PII: S1773-2247(25)00372-7

DOI: https://doi.org/10.1016/j.jddst.2025.106969

Reference: JDDST 106969

To appear in: *Journal of Drug Delivery Science and Technology*

Received Date: 6 November 2024

Revised Date: 15 April 2025

Accepted Date: 23 April 2025

Please cite this article as: A.O. Al Khatib, A. Yousfan, A. Abed, M. El-Tanani, H. Al-Obaidi, Development of pimozide spray dried lipid nanoparticles with enhanced targeting of non-small cell lung cancer, *Journal of Drug Delivery Science and Technology*, https://doi.org/10.1016/j.jddst.2025.106969.

Development of pimozide spray dried lipid nanoparticles with enhanced targeting of non-small cell lung cancer

Arwa Omar Al Khatib[b], Amal Yousfan[a], Anas Abed[b], Mohamed El-Tanani[b,c], Hisham Al-Obaidi[a]*

a) School of Pharmacy, University of Reading, Reading RG6 6AD, UK
b) Faculty of Pharmacy, Al Ahliyya Amman University, Amman 19111, Jordan
c) College of Pharmacy, RAK Medical and Health Sciences University, Ras Al Khaimah P.O. Box 11172, United Arab Emirates

*Address correspondence to Hisham Al-Obaidi, h.al-obaidi@reading.ac.uk

Abstract

This study aims to develop and evaluate the pimozide-loaded lipid nanoparticles (LNPs) designed for the targeted treatment of non-small cell lung cancer (NSCLC). Employing the microemulsion technique, three distinct types of LNPs were synthesized: solid lipid nanoparticles (SLN), nanostructured lipid carriers (NLC), and liquid lipid carriers (LLC). These formulations were optimized in order to transform them into fine powders through spray drying. An assessment of their encapsulation efficiency (EE%), particle size, moisture sorption, surface morphology, and anti-proliferative activity against A549 lung cancer cells were evaluated. NLC formulations exhibited the highest EE% at approximately 96% ±2.1%, attributed to the inclusion of oleic acid, which disrupted the lipid matrix's crystalline structure to enhance drug encapsulation. In contrast, SLN formulations demonstrated the lowest EE%, with values barely exceeding 70% ±2.5%, highlighting the limitations of their solid lipid content. The spray drying process significantly altered the particle sizes, transitioning them from nano to microscale and resulting in a modest decline in EE% across all LNP types. Further, DVS analyses highlighted the moisture sorption capabilities of the LNPs, showing diverse trends among the formulations. LLCs demonstrated the highest sorption capacity, suggesting a highly porous structure. FTIR spectroscopic analysis revealed specific interactions between the drug and lipid matrix, indicating successful encapsulation. Raman spectroscopy further confirmed the uniform distribution of pimozide and excipients within the LNPs and highlighted how oleic acid and PEG-400 co-localize, crucial for boosting drug loading capabilities. X-ray powder diffraction (XRPD) analysis showed varying degrees of crystallinity across the formulations, with LLCs exhibiting the most amorphous nature followed by NLCs and then SLNs. Surface morphology studies through SEM analysis showed the transformation from nanoparticles to microparticles post spray drying, with distinct textural differences among the formulations. The anti-proliferative activity against A549 cells identified NLC 4, NLC 5, and LLC 5 as particularly effective, with IC50 values notably lower than that of free PMZ, highlighting improved therapeutic potential. Drug release studies revealed a biphasic release pattern for the promising formulations, offering sustained drug availability, crucial for effective NSCLC treatment.

1. Introduction:

Lung cancer continues to pose a health challenge contributing to a substantial number of cancer related deaths. Non-small cell lung cancer (NSCLC) a type, within the spectrum of lung cancers accounts for around 85% of all cases [1]. The complexity of this subtype becomes apparent in advanced stages of diagnosis. Traditional treatment methods like surgery, chemotherapy and radiation therapy often show effectiveness during these stages. With treatments facing constraints there is a growing emphasis on exploring therapeutic approaches. This shift is primarily motivated by the pursuit of less harmful treatment alternatives. Among the emerging strategies gaining attention is drug repurposing, which offers benefits such as quicker and cost effective pathways to clinical implementation due, to the extensive safety and efficacy testing these drugs have already undergone in their original applications [2].

In this context, the use of the antipsychotic drug pimozide (PMZ), has emerged as a candidate for repurposing due to recent discoveries of its anticancer properties [3]. Originally prescribed for psychiatric conditions, the efficacy of Pimozide against various cancer cell lines—including lung, liver, leukemia, breast, prostate, and brain cancers—has prompted a reassessment of its potential in treating NSCLC.

The interest in pimozide for NSCLC treatment is driven by its established safety profile, minimal adverse effects, and affordability, which are advantageous in the context of drug repurposing [4]. Such attributes make pimozide a compelling option in the development of new therapeutic strategies, particularly for lung cancer, where the precision of drug delivery is paramount. Ensuring that PMZ reaches the tumour location effectively is crucial for maximizing its therapeutic impact while minimizing the potential side effects that are often associated with the systemic distribution of anticancer drugs.

The main obstacle lies in ensuring that PMZ reaches the tumour location effectively maximizing its impact on cancer cells while minimizing side effects commonly linked with widespread distribution of drugs throughout the body. This accomplishment is significant due to the precision needed to target cancer cells and navigate the environment within tumour sites.

In addressing this challenge, the use of lipid nanoparticles (LNPs) as a delivery mechanism is of a great importance. LNPs offer several advantages, such as enhancing drug solubility, stability, and bioavailability [5]. They provide a protective encapsulation for the drug, preventing against premature degradation and facilitating a more controlled release at the target site [6]. This targeted delivery is especially essential in cancer treatment to minimize systemic exposure to potent medications, thereby reducing side effects [7]. The consideration of different types of LNPs presents a tailored approach to optimize pimozide's delivery.

Solid Lipid Nanoparticles (SLN) consist of solid lipids and create a stable matrix, conducive for a controlled drug release. Their solid state at body temperature aids in maintaining the integrity of PMZ, ensuring sustained effectiveness. Nanostructured Lipid Carriers (NLC), on the other hand, blend both solid and liquid lipids. This combination yields a more complex matrix, potentially allowing for a higher drug load and a more customized release profile [8]. Recent research by Al-Haj et al. (2024) highlights the potential of PMZ-loaded NLCs. The resulting NLCs demonstrated pH-sensitive release, enhancing tumour-specific delivery, and showed superior anticancer activity on A549 cell lines compared to free PMZ, with an IC50 of 12.9 μM for PMZ-NLC versus 16.5 μM for free PMZ [9]. Lastly, we have explored the single use of liquid lipids in nanoparticle formulation referred to as Liquid Lipid Carriers (LLC). This strategy, which is primarily composed of liquid lipids, could offer distinct characteristics such as improved drug solubility and potentially quicker release rates. This could be advantageous for rapidly achieving therapeutic concentrations of PMZ at the tumour site. Such level of customization in drug delivery could therefore aid in advancing the treatment of NSCLC.

Spray drying is widely used for formulating powders of fine particle sizes that are essential for effective lung deposition [10]. When dealing with respiratory diseases like NSCLC, ensuring that the drug reaches the deeper regions of the lungs is necessary for effective treatment [11]. This is where Dry Powder Inhalers (DPIs) become important. DPIs are increasingly favoured in pulmonary drug delivery due to their efficiency in delivering medication directly to the lungs [12]. Using spray drying, PMZ -loaded lipid nanoparticles can be transformed into a fine powder suitable for DPIs. This powder must have the right

particle size distribution to ensure deep lung penetration, optimizing the drug's therapeutic effect on lung cancer cells.

The control over particle size, density, and morphology during spray drying is critical [13], as it directly impacts the drug's deposition in the lungs. In the case of PMZ formulations for NSCLC, the use of lipid matrices, such as stearic and oleic acids, and surfactants like Poloxamer 407 and PEG 400, provide the foundational stability [14]. These components help maintain the integrity of the particles and ensure consistent drug release. Additionally, this study introduces the use of stabilizers, such as conventional sugars like isomalt and trehalose which have been traditionally used as stabilizers, and protectants [15].

The aim of this study is to develop and optimize spray-dried pimozide-loaded lipid nanoparticles (SLNs, NLCs, and LLCs) for targeted NSCLC therapy, evaluate their physicochemical properties, drug release profiles, and in vitro anticancer efficacy, and establish their potential as a pulmonary drug delivery system.

2. Materials and methods:

2.1 Materials

Pimozide, stearic acid, oleic acid, poloxamer 407, PEG 400, and trehalose used in this study were purchased from Sigma-Aldrich- USA. While the methocel E5 (HPMC E5) was obtained from DuPont, Netherlands. Isomalt was purchased from BENEO GmbH, Germany, and OraRez PVM/MA copolymer, an alternating copolymer of methyl vinyl ether and maleic anhydride was obtained from HARKE Pharma GmbH, Germany. Finally, the MTT reagent was purchased from ThermoFisher Scientific, USA, and Dimethyl sulfoxide (DMSO) was obtained from Fisher Bioreagents, USA.

2.2 Preparation of lipid nanoparticles with different types of lipids

The microemulsion method was employed to create all lipid nanoparticles using different kinds of lipids. The optimized quantities of all ingredients including PMZ, stearic acid, oleic

acid, polymer, and surfactants are indicated in Table 1. Excipients were incorporated at approximately a 5% ratio to serve as stabilizers and protectants [16].

This method combines oil, water, and surfactants, utilizing them to stabilize tiny droplets within another liquid. To prepare Lipid Nano Particles (LNPs), 50 mg pimozide was dissolved in the lipid phase—200 mg stearic acid for Solid Lipid Nanoparticles (SLNs), 100 µL oleic acid for Liquid Lipid Carriers (LLCs), or a combination of 100 mg stearic acid and 100 µL oleic acid for Nanostructured Lipid Carriers (NLCs)—at 85°C. The lipid phase volume was 1 mL. The aqueous phase consisted of 200 mg Poloxamer 407 and 100 µL PEG 400 dissolved in 50 mL water, with the aqueous phase volume being 50 mL. Both phases were heated to 85°C, above their Phase Inversion Temperature (PIT), facilitating the transformation from a microemulsion to a stable nanoparticle dispersion. The phases were then vigorously mixed at this temperature. After cooling, 300 mg HPMC-E5 and 60 mg of one of the excipients (trehalose, OraRez, or isomalt) were added with continuous stirring. The final nanoparticle suspension volume was 50 mL. The concentration of pimozide in the final feed solution was 1 mg/mL. The resulting nanoparticle dispersion was then spray-dried to obtain the final powder formulation.

2.3 Preparation of spray- dried powders

A Büchi mini spray dryer B-290, from Büchi Labortechnik AG in Falwil, Switzerland, was used to transform SLN, NLC, and LLC nanosuspensions into fine dry powders. The process involved feeding the solution into a two-fluid nozzle for spray drying under specific conditions: a nitrogen gas flow of 50 mL/min, an inlet temperature of 120 °C (± 2 °C), an outlet temperature of 70 °C (± 2 °C), a feed flow rate of 2.4 mL/min, and the aspirator blower operating at full capacity.

Table 1: Composition of spray- dried pimozide- loaded lipid microparticles' formulations

	PMZ (mg)	Stearic acid (mg)	Oleic acid (µL)	Poloxamer 407 (mg)	PEG 400 (µL)	HPMC-E5 (mg)	Yield%	Excipients (mg)		
								Trehalose	OraRez	Isomalt
SLN 4	50	200	-	200	100	300	71.3	60	-	-
SLN 5	50	200	-	200	100	300	70.1	-	60	-
SLN 6	50	200	-	200	100	300	69.5	-	-	60
NLC 4	50	100	100	200	100	300	88.8	60	-	-
NLC 5	50	100	100	200	100	300	91.1	-	60	-
NLC 6	50	100	100	200	100	300	88.5	-	-	60
LLC 4	50	-	100	200	100	300	88.5	60	-	-
LLC 5	50	-	100	200	100	300	89.4	-	60	-
LLC 6	50	-	100	200	100	300	87.9	-	-	60

2.4 Encapsulation Efficiency (EE%)

To evaluate how well the PMZ was trapped, the LNPs containing PMZ were separated from the LNPs suspension through centrifugation, at 25,000 rpm for half an hour. Following this, 10 mL of the supernatant was mixed with 10 mL of methanol. A 1 mL sample of this mixture was then taken, and the amount of PMZ in this solution was measured using HPLC.

For the quantification of Pimozide content within the spray dried LNPs, an HPLC method described by Al-Haj et al. (2024) was utilized [9]Brefly, 10 mg of each powder was dissolved in 10 mL of methanol. Then spun it at 13,000 rpm, for half an hour. After that the supernatant was filtered through 0.22 µm filters. Analysed the PMZ content using HPLC. The analysis was done using a C18 column that was 15 cm long with detection at

a wavelength of 270 nm. Our mobile phase for HPLC consisted of 45% acetonitrile, and 55% water with pH adjusted to, around 2.5 using an amount of phosphoric acid. An isocratic elution method was employed with a flow rate of 1mL/min, injection volume of 20 µL, and run time of 10 minutes. Calculated the pimozide concentration based on the Area Under the Curve (AUC) derived from our HPLC data through a calibration curve created by linear regression. The percentage of encapsulation efficiency (EE%) was calculated using a specific formula:

$$EE\% = \frac{PMZ_{Total} - PMZ_{Supernatant}}{PMZ_{Total}} \times 100\%$$

2.5 Particle size and zeta potential measurements

In this study, the average particle size of the prepared PMZ- loaded LNPs' nanosuspensions and spray- dried powders were determined using the dynamic light scattering (DLS) (a Zetasizer Nano ZS, (Malvern Instruments, UK). For determining zeta potential, the Malvern Zetasizer instrument used in our study employs laser Doppler electrophoresis. This technique analyses the motion of particles under an electric field to determine their surface charge. Briefly, 100-fold dilution of LNP nanosuspensions was prepared using distilled water.

For the preliminary assessments and the stability analysis following a two-month storage period at room temperature (20°C to 25°C) in a desiccator, 5 mg of each spray-dried LNP powder was first re-dispersed in 5 mL of distilled water. A 10 µL sample from this dispersion was further diluted to a final volume of 1000 µL with distilled water. The resulting dispersions were then placed into a glass cuvette and subjected to measurements under controlled conditions, which included a temperature set at 25 °C, a refractive index fixed at 1.33, and a measurement duration of 60 seconds. Average particle size, and zeta potential were performed in triplicate.

2.6 Dynamic Vapor Sorption (DVS) measurements

The moisture interaction and physical stability of the pimozide-loaded lipid nanoparticles (LNPs) were investigated using Dynamic Vapor Sorption (DVS) analysis. The DVS experiments were conducted on a Discovery Sorption Analyzer (Discovery SA) system (TA Instruments, USA), equipped with a vertical nulling microbalance. This setup allows for precise control over temperature and humidity conditions, essential for assessing the hygroscopic properties of the LNPs.

The DVS procedure was designed to evaluate the moisture sorption and desorption behaviour of the LNPs under controlled conditions. Initially, the system was equilibrated at 25 °C with a humidity setting of 0 %RH. To ensure the capture of significant moisture interactions, the experiment was programmed to abort the next segment if the percentage weight change was less than 0.01% for a duration of 10.0 minutes.
Following the equilibration, the sample underwent an isothermal hold for 1440.0 minutes (24 hours) to stabilize under the initial conditions. The humidity was then incrementally increased in steps of 10 %RH every 1440.0 minutes, progressing from 0 %RH to 90%RH.

Each humidity step was subjected to the same abort condition if the percentage weight change was less than 0.01% for 10 minutes, ensuring that the measurements reflected meaningful moisture uptake or release. The experiment also included a desorption phase, where the humidity was stepwise decreased from 90 %RH back to 0 %RH under the same conditions and abort criteria, allowing for a comprehensive analysis of the LNPs' moisture interaction characteristics.

2.7 Fourier Transform Infrared spectroscopy (FTIR)

Fourier transform infrared (FTIR) spectra measurements were collected for all spray-dried samples using a Perkin-Elmer Spectrum 100 (Waltham, MA, USA) spectrophotometer, over a scan range of 650–4200 cm^{-1} with an average of 16 scans.

2.8 Raman spectroscopic analysis

Separate measurements of the various components constituting the spray-dried LNPs' powders were collected by simply placing a few grains of each sample on a microscope slide and scanned using LabRAM Soleil™ confocal Raman microscope (Horiba Scientific, Kyoto, Japan). The powders were found in the microscope using a low magnification lens and then after switching to a 50X objective a representative location was selected from a full focus ViewSharp™ image.

Spectra were acquired with the 532nm laser, 600 g/mm grating, 50X long working distance lens, 67 mW laser power at the sample and 10 second acquisition time. Measurements were taken at multiple locations to ensure that a representative spectrum was used for each sample. The only exceptions to this were the pimozide sample that was damaged by this high laser power so 17mW was used for a total of 20 seconds to give a comparable signal level. Similarly, the OraRez sample exhibited some fluorescence so a 20 second acquisition was used after illuminating the sample with laser light for 60 seconds to quench the fluorescence. An alternative laser could have been used but the 532 nm was selected to allow direct comparison with the map data.

A ViewSharp™ image was taken and the topography information used to rapidly autofocus at every point on the map. This allowed the system to be used in moderate confocality mode (100 µm pinhole) without any significant variation in signal level. Each map covered a 100 µm by 90 µm area with 1 µm step size. To analyse the maps, multivariate CLS (classical least squares) algorithm was used. The spectra of the applicable constituents were used as loadings and the fitting coefficients were plotted as maps to show the location of each component.

2.9 X- ray powder diffraction (XRPD)

X-ray powder diffraction analysis was carried out using Bruker D8 Advance flat plate powder diffractometer (Bruker AXS GmbH, Germany). The samples were irradiated with copper source radiation (1.54A° angstroms). The data collection was carried from 5.0° to 90.0134° 2theta, 0.27646647° step size at 1.2 seconds per step.

2.10 Scanning Electron Microscopy (SEM)

The shape, surface, morphology, and microstructure of the particles were examined using SEM (Scanning Electron Microscopy) (Microscope: FEI Quanta 600 FEG SEM) (FEI Co. Inc., Hillsboro, Oregon). The produced microparticle samples were mounted on aluminium stubs with double-sided adhesive carbon tabs (Leit Adhesive Carbon Tabs 12mm Dia (Pack of 100)-Code: SP12-Supplier: EM Resolutions) (Pin stub 12.5mm (Aluminium) with groove (8mm pin) (pack of 100)-Code: SP12-Supplier: EM Resolutions)-Supplier: Agar Scientific-Code: AGG3347N). Carbon fibre was applied to all samples twice. To gold coat the samples for photos taken under high vacuum, an Edwards Sputter Coater S150B was used. All specimens were then photographed at different magnifications ranging from 100X to 10000X using an accelerating voltage of 20 kV.

2.11 Cell culture work and MTT cell viability assay

2.11.1 Cell culture

The A549 cancer cell model was used during the course of this study. Those cells were cultured and maintained in a Roswell Park Memorial Institute (RPMI) growth media (Euroclone, Italy) supplemented with 10% Fetal Bovine Serum (FBS) and 1% penicillin/streptomycin (Gibco). The cells were maintained at 37°C and 5% CO_2 in a humidified incubator.

2.11.2 MTT cell viability assay

Cell viability was evaluated using the MTT assay. Briefly, A549 lung cancer cells were seeded at a density of $5x10^3$ cells per well in a 96-well plate which was subsequently incubated overnight to allow cell adhesion. Next day, cells were treated with various concentrations of PMZ, ranging from 0.3125-200 μM, or equivalent concentrations of each formulation, specifically the formulations that have exhibited a potential antiproliferative activity post the preliminary screening of all formulations, namely NLC4, NLC5, and LLC5, or blank excipients for a duration of 72 hours.

At the designated time point, each well was treated with 0.5 mg/mL of MTT reagent, and the plate was incubated for an additional 3 hours to facilitate the formation of formazan crystals. Subsequently, 100 µL of DMSO was added to each well to dissolve the formazan crystals. Finally, the absorbance was measured at 570 nm using a BioTek Cytation 5 multi-mode plate reader (USA). The results of cell viability were expressed as a percentage relative to the untreated control group.

2.12 Drug release study

Three formulations, in particular these having potential IC50 values, were evaluated to assess the PMZ release: NLC4, NLC5, and LLC5. Briefly, 10 mg of each spray-dried formulation was resuspended in 5 mL of simulated lung fluid (SLF) which is composed of (100 mM NaCl, 5 mM KCl, 2 mM CaCl2, 25 mM NaHCO3, 5 mM Na2HPO4, 1 mM NaH2PO4, 1 mM MgCl2 hexahydrate, pH = 7.4).

This suspension was immediately enclosed within a dialysis bag, which was subsequently immersed in a vial containing 20 mL of SLF under constant stirring at 800 rpm at 37°C. To monitor the PMZ release, 1 mL of the SLF containing the released PMZ was extracted from the vial at regular time intervals. Simultaneously, to ensure sink conditions, an equivalent volume of fresh SLF was added back into the system. These collected samples were then analyzed using HPLC utilizing a 5 cm C18 column with detection at 270 nm and an isocratic method comprising a 45:55 acetonitrile: water mobile phase and the cumulative drug release from each formulation was calculated. The release kinetic of free pimozide was also monitored and used as a control.

2.13 Statistical analysis

In order to compare the variations, between formulations we used a one-way analysis of variance (ANOVA) with Pythons SciPy library. All statistical analyses were carried out with significance levels set at *$p < 0.05$, **$p < 0.01$, and ***$p < 0.001$, with a minimum sample size of $n = 3$.

3. Results and discussion

In this study, three types of PMZ-loaded lipid nanoparticles were developed: solid lipid nanoparticles (SLN), nanostructured lipid carriers (NLC), and a unique formulation that only uses liquid lipids, named as liquid lipid carriers (LLC). Spray drying transformed these lipid nanoparticles into a powdered form, causing them to shift from nanoscale to microparticle size. Following this transition, thorough physicochemical analyses of the spray-dried microparticles were conducted.

3.1 Encapsulation efficiency of spray dried particles

Figure 1(A) presents the encapsulation efficiency percentages (EE%) of nine spray-dried LNP formulations, highlighting the impact of formulation composition on EE%. Notably, NLC5 achieves the highest EE% at approximately 96%± 1.1%, likely due to the addition of oleic acid, which disrupts the solid lipid's crystalline structure and enhances the lipid matrix's drug entrapment capacity [17]. The incorporation of liquid lipid also aids in preventing drug expulsion, significantly improving EE% compared to SLNs [18]. This improvement is further supported by the reduced particle size in NLC formulations as discussed in Section 3.2, which provides a greater surface area relative to volume, enhancing drug-lipid interactions and stabilization within the formulations.

Conversely, SLN6 shows the lowest EE% at just over 70%± 3.4%, attributed to the rigid and crystalline nature of its solid lipid component, stearic acid, which tends to expel the drug during the cooling phase, thereby reducing EE% [18]. This expulsion of the drug is a common issue in highly ordered crystal lattices, which diminishes encapsulation efficiency [19]. Despite this, other NLC and LLC formulations exhibit significantly higher EE%, emphasizing the crucial role of lipid matrix composition in drug encapsulation. Table 1 indicates that variations within individual formulations (e.g., SLN4, SLN5, SLN6) are mainly due to different excipients used, accounting for only about 5% by weight of the overall formulation, showing a consistent EE% across groups.

The encapsulation efficiency (EE%) data shows that the mean EE% values for SLNs, NLCs, and LLCs are 74.0%, 94.2%, and 93.3%, respectively. This indicates that for SLNs,

about 74.0% of the drug is encapsulated within the lipid nanoparticles, while for NLCs and LLCs, the encapsulation efficiency is significantly higher, with 94.2% and 93.3% of the drug being entrapped. High encapsulation efficiency is crucial as it enhances drug stability and protects it from degradation, ensuring sustained release and improved bioavailability. The relatively small percentage of free drug (26.0% for SLNs, 5.8% for NLCs, and 6.8% for LLCs) suggests efficient encapsulation, which minimizes the risk of rapid degradation or premature release, maintaining therapeutic drug levels over an extended period. Thus, achieving high EE% is essential for optimizing the formulation's effectiveness and ensuring the drug's stability and controlled release profile.

Figure 1(B) further compares EE% across different formulations. NLCs show a mean EE% of 94.2%± 2.10%, closely followed by LLCs at 93.3%± 1.00%. An ANOVA test confirms no statistically significant difference between these groups (p-value > 0.05). However, a comparison of SLNs against NLC and LLC groups reveals a notable statistical difference, with SLNs exhibiting a significantly lower mean EE% of 74.0%± 2.50%, underscoring the superior drug encapsulation capabilities of NLC and LLC formulations due to their lipid matrix properties. This finding is supported by previous research [20, 21], showing that incorporating liquid lipid into the matrix, as evidenced by XRPD data in Section 3.5, introduces imperfections into the crystalline structure, thereby increasing the space available for drug encapsulation [17] and preventing drug expulsion.

All types of LNPs experienced a reduction in EE% following spray drying. For SLNs, EE% decreased from 78.0% ± 1.80% to 74.1% ± 2.50%, indicating moderate vulnerability to the thermal and mechanical stresses of the drying process. Similarly, NLCs and LLCs exhibited slight decreases in EE%, with the drying process impacting their EE% minimally. These decreases can be attributed to the rapid evaporation of solvent during drying, altering the solubility and distribution of lipids, often leading to LNPs' aggregation or fusion and resulting in larger particle sizes with a greater surface area to volume ratio [22]. These effects are more pronounced in formulations with higher proportions of crystalline lipids, such as SLNs, while the incorporation of liquid lipids in NLCs and LLCs mitigates these disruptions. Additionally, the high temperatures involved in spray drying can alter the lipid

composition and induce changes in the crystallinity of lipid components, further compromising the physical stability and integrity of the nanoparticles [23].

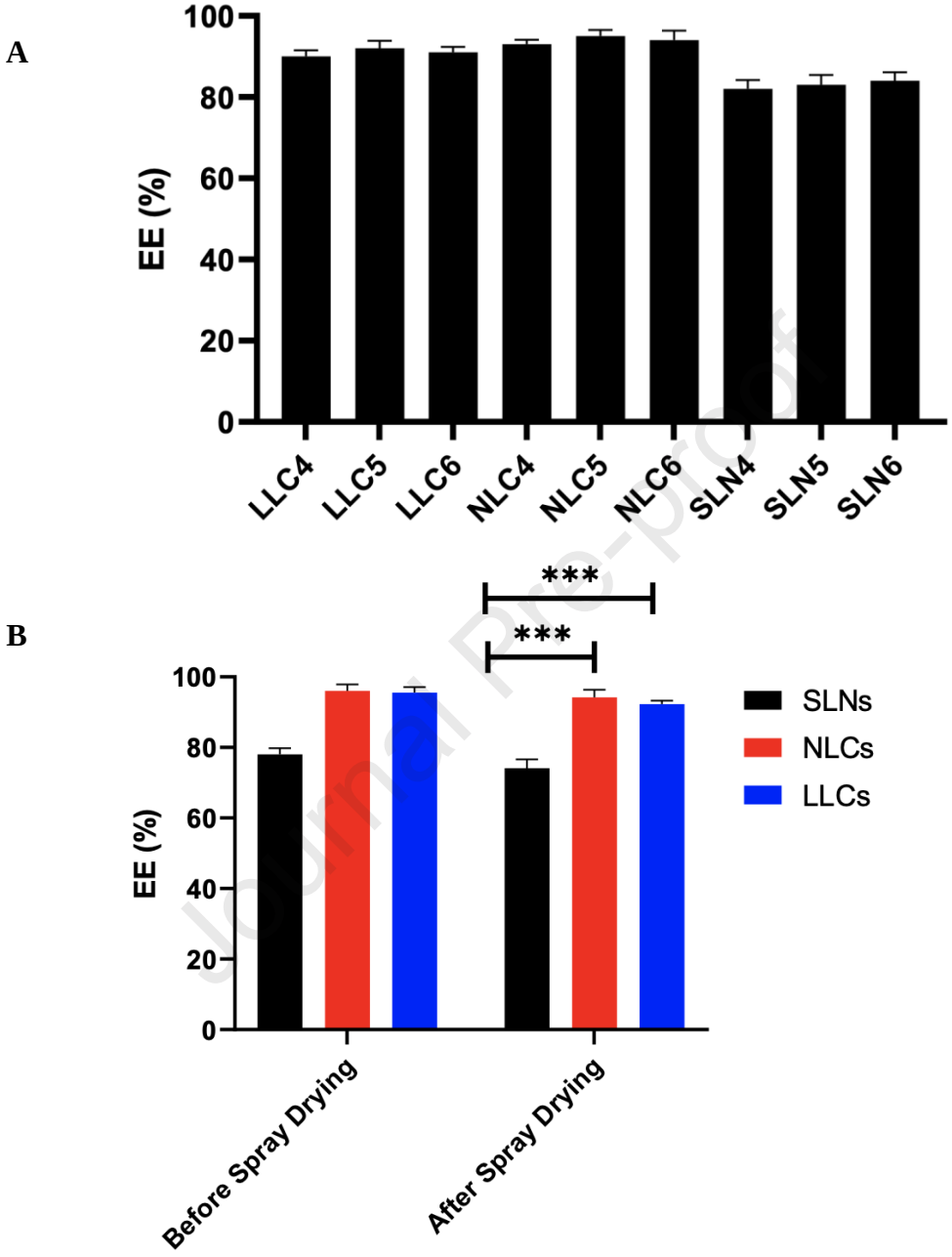

Figure 1. Bar graph shows **(A)** Encapsulation Efficiency (EE%) of nine spray dried lipid nanoparticles (LNPs) with error bars showing the deviation (± SD) and **(B)** mean EE (%) for SLNs (black), NLCs (red), and LLCs (blue), before and after spray drying. Each bar represents the average of multiple formulations per type. (***) indicates $p < 0.001$ showing statistical significance, n = 3.

3.2 Particle size and zeta potential

The impact of spray drying on the particle size of nine PMZ-loaded lipid nanoparticles, classified as SLN, NLC, and LLC, was investigated, with a detailed measurement and analysis of particle sizes before and after spray drying. **Figure 2(A)** reveals notable differences in particle sizes across SLN, NLC, and LLC formulations, largely attributed to the unique lipid characteristics of each. In SLNs, the rigid, crystalline nature of stearic acid may hinder efficient drug encapsulation, resulting in larger or more variably sized particles. Conversely, NLC formulations, blending stearic and oleic acids, disrupt the crystalline structure, leading to a partly amorphous/crystalline matrix that better incorporates PMZ and yields smaller particles. However, spray-dried LLC formulations, due to their pure liquid lipid systems, exhibited larger particles than NLCs. This could be due to lower viscosity, which might promote the coalescence of droplets leading to larger particle sizes. This effect is compounded by the surfactant stabilization possibly being less effective in the uniform liquid lipid phase of LLCs, failing to prevent the growth of larger particles. The absence of solid lipids in LLCs delays nucleation and solidification, allowing more time for particles to grow or coalesce, resulting in the observed larger particle sizes [24].

A significant increase in particle sizes across all formulations post-spray drying is indicated in **Figure 2(A, B)**, where a transition from nano to micro-scale was evident. Initially, LNPs were within the nano-sized range but post-spray drying there was a pronounced shift to the microparticle range. This increase primarily results from heating-induced phase transitions and aggregation due to particle interactions, indicating a high likelihood of particle aggregation or fusion during drying, influenced by factors such as drying temperature, shear stress, or the physicochemical properties of the lipids and drug [22, 25].

PMZ-loaded SLNs, predominantly composed of stearic acid, are notably affected during spray drying. The properties of stearic acid, with its higher melting point and rigid structure, lead to significant aggregation and fusion due to melting and recrystallization under spray drying conditions [26]. This effect is particularly pronounced in formulations relying solely on solid lipids. In contrast, PMZ-loaded NLCs, which blend solid stearic acid and liquid oleic acid, experience less particle aggregation and fusion, benefiting from the fluidity of oleic acid. This blend results in a less organized lipid matrix, more effectively

encapsulating the drug and limiting particle size growth. Similarly, PMZ-loaded LLCs, solely containing liquid oleic acid, show smaller size increases post-drying due to the highly flexible matrix that better withstands drying.

The impact of particle size on the drug delivery of inhaled chemotherapy was addressed in our recently published review article [27]. It was detailed that the optimal particle size for inhaled chemotherapeutic agents lies within an aerodynamic diameter range of 1–5 μm. Particles within this size range are ideally suited for penetrating the deeper regions of the lungs, thereby enhancing therapeutic outcomes for treatments targeted at lung-specific ailments. Conversely, particles larger than 5 μm are generally not able to alter their trajectory within the airflow and are typically deposited in the upper airways through inertial impaction. Particles smaller than 1 μm, on the other hand, tend to remain suspended in the airstream and are likely to be exhaled, with diffusion being the predominant mechanism of deposition when they settle. This size-dependent behavior emphasizes the importance of careful design in particle size to optimize delivery efficiency and therapeutic efficacy in pulmonary drug delivery systems

A

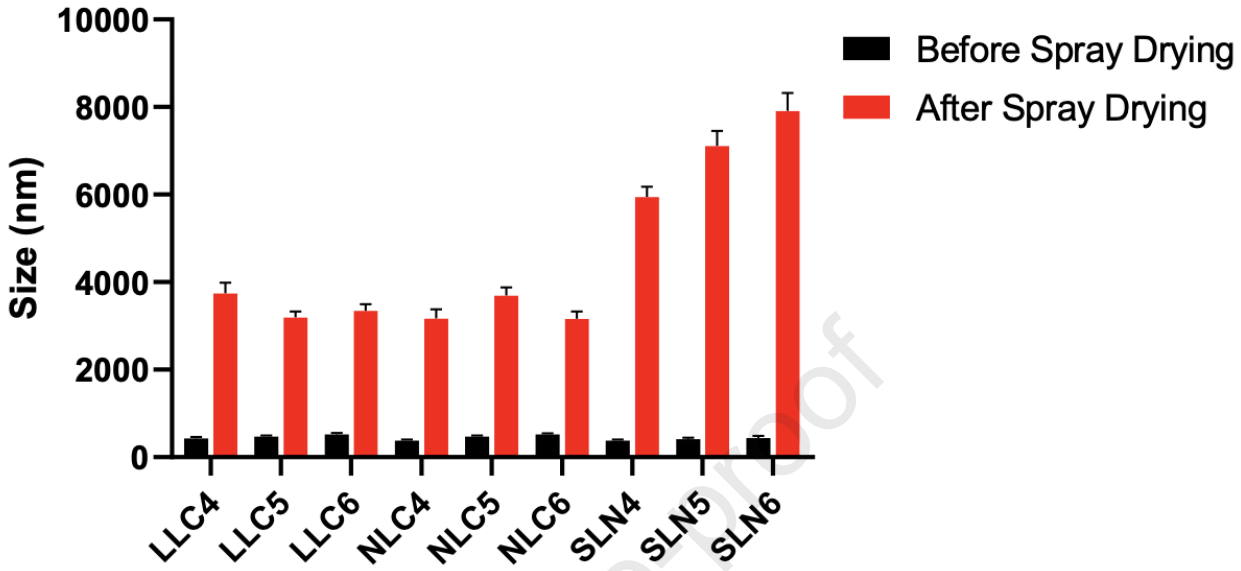

B

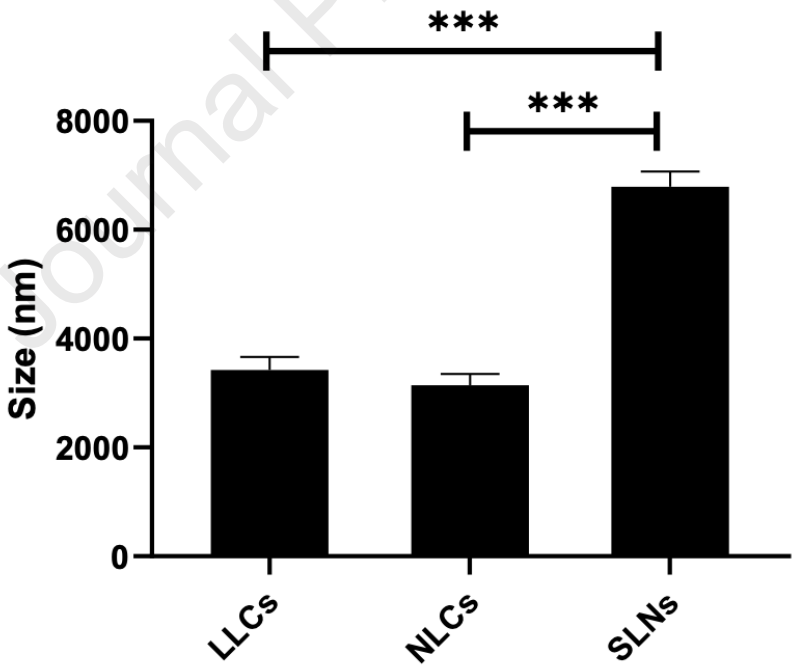

Figure 2. (A) Particle size measurements for spray-dried LNPs before and after spray drying. **(B)** Comparative analysis of particle sizes within three categories of spray-dried LNPs loaded in which each bar represents the average of multiple formulations per type. (***) indicates $p < 0.001$ showing statistical significance, n = 3.

The zeta potential of all lipid nanoparticle formulations was found to be negative, influenced by the incorporation of negatively charged stearic acid in the SLN and NLC formulations [28] , and further amplified by the addition of oleic acid in the NLC and LLC formulations [29]. This negative charge is advantageous, especially for targeted therapy in NSCLC, as it can potentially enhance evasion from immune detection, reduce clearance rates, and prolong circulation time in the bloodstream [30].

Figure 3 shows a statistically significant reduction in the zeta potential of all lipid nanoparticle types following spray drying, indicating changes in surface charge characteristics. This decrease in negative charge was observed across SLN, NLC, and LLC formulations (e.g., SLN4–6, NLC4–6, LLC4–6), and may be attributed to partial degradation or reduced adsorption of non-ionic surfactant stabilizers at elevated spray drying temperatures, leading to weaker electrostatic repulsion [31]. Among the formulations, NLCs retained the highest stability with an average zeta potential of –33.0 ± 2.9 mV, followed by SLNs at –22.0 ± 8.3 mV, suggesting moderate stability. LLCs showed the lowest stability with a zeta potential of –14.1 ± 1.4 mV, approaching the range where particle aggregation is more likely.

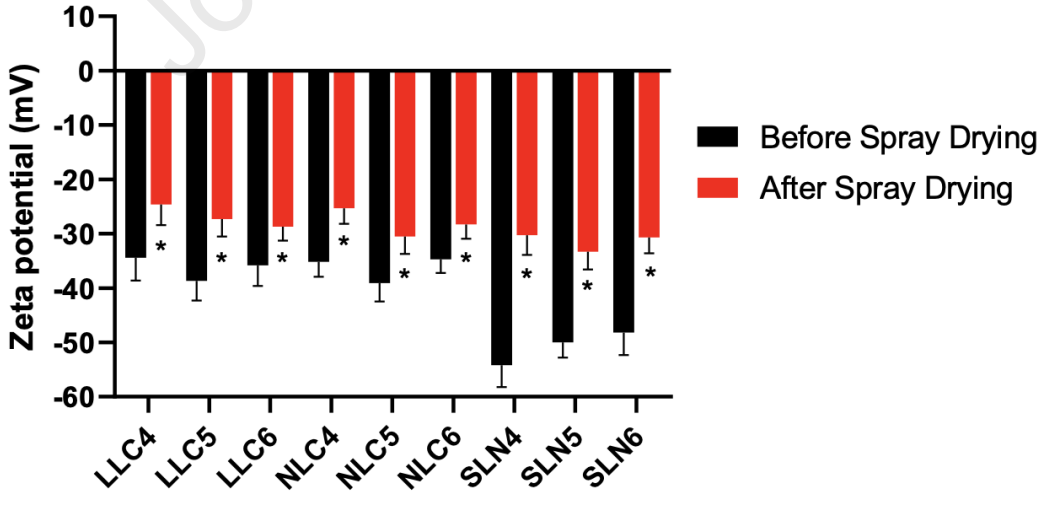

Figure 3. Average zeta potential before and after spray drying nine spray-dried LNPs. Statistical significance is indicated by *$p < 0.05$, n = 3.

Stability studies of PMZ-loaded LNPs were conducted by assessing the average particle size and zeta potential after storage at room temperature (20°C to 25°C) in a desiccator for 2 months. The results, displayed in **Figure 4 (A)**, show a trend of maintained or slightly increased particle size, indicating moderate size stability or minor aggregation over time. Specifically, LLC formulations (LLC4, LLC5, LLC6) demonstrated a modest increase in average size, remaining within the standard deviation of initial measurements, suggesting stable nano-systems with slight aggregation. In contrast, NLC formulations (NLC4, NLC5, NLC6) showed more consistent size stability, attributed to their inhibition of the recrystallization process in solid lipids, maintaining size consistency over the storage period [32]. However, SLN formulations (SLN4, SLN5, SLN6) exhibited a more pronounced size increase, indicating a greater tendency towards aggregation or particle growth, possibly due to lipid crystallization within the SLN structure leading to drug expulsion and increased particle size [33].

Figure 4 (B) presents zeta potential changes post-storage, revealing a notable decrease for LLC formulations (LLC4, LLC5, LLC6), suggesting less stability, likely exacerbated by moisture sensitivity as confirmed by DVS results in Section 3.3. This reduction in zeta potential may also be influenced by the Ostwald ripening effect, where smaller particles dissolve and redeposit onto larger ones, altering particle size distribution and decreasing zeta potential [34]. Conversely, NLC formulations showed minimal changes in zeta potential, maintaining more negative charges and indicating enhanced stability. SLN formulations (SLN4, SLN6), however, showed significant declines in their zeta potential, likely due to particle aggregation affecting the density of surface charge and lowering the negative zeta potential [35].

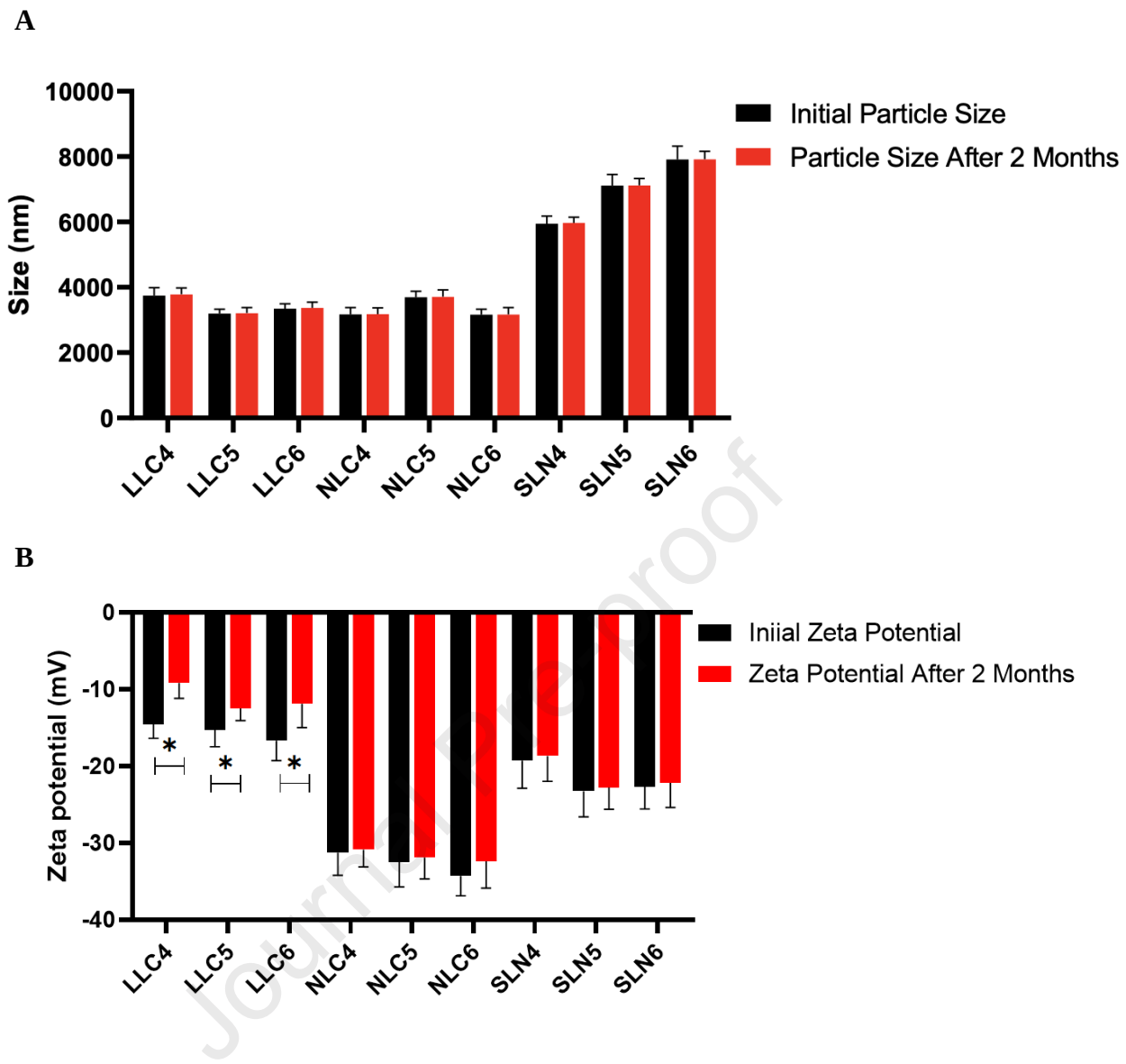

Figure 4. (A) The average size stability of SLN, NLC and LLC formulations before and after storage. **(B)** Zeta values before and after storage. Statistical significance is indicated by *$p < 0.05$, n = 3.

3.3 Analysis of moisture sorption using Dynamic Vapour Sorption (DVS)

The study investigated the sorption behavior of relative humidity (RH%) across three representative LNP formulations: one solid lipid nanoparticle (SLN), one nanostructured lipid carrier (NLC), and one liquid lipid carrier (LLC). Despite similar encapsulation efficiencies, the sorption trends varied significantly among these formulations due to differences in their lipid compositions. **Figure 5 (A)** details SLN4's gradual and controlled moisture interaction, with a peak weight increase of 35% at high RH levels, indicating

diffusion through a denser or less porous matrix. Interestingly, a decrease in sorption during a second cycle at 70% RH suggests potential crystallization within the matrix.

In contrast, NLC5 exhibited a more dynamic response to humidity as depicted in **Figure 5 (B)**. Initially, when RH% increased from 0% to about 80%, NLC5's weight quickly rose, peaking at 12%. This rapid weight gain doubled beyond 80% RH, reaching 25%, reflecting a highly porous internal structure capable of swift moisture adaptation.

LLC5's response, shown in **Figure 5 (C)**, was the most variable, with significant weight fluctuations up to 42% at similar RH levels, indicating a high sorption capacity. This was likely due to its liquid lipid composition, primarily oleic acid, which allows for more mobile and substantial moisture interactions. The pronounced fluctuations during the desorption phase, not mirrored in subsequent cycles, suggest an irregular pore distribution within LLC5, leading to differential rates of moisture absorption and release. This highlights the complex interaction between LLC5's unique composition and environmental moisture, underscoring the distinct sorption characteristics of each LNP type under varying humidity conditions.

The distinct moisture interaction behaviours observed among SLN4, NLC5, and LLC5 formulations can be attributed to their specific lipid compositions and stabilizers. SLN4, comprising only solid stearic acid lipid and trehalose, exhibits a gradual and controlled moisture interaction, peaking at a 35% weight increase at high RH levels. This suggests diffusion through a denser or less porous matrix, with a decrease in sorption during a second cycle at 70% RH indicating potential crystallization within the matrix. NLC5, which includes a combination of solid stearic acid lipid, liquid oleic acid, and OraRez, shows a more dynamic response to humidity. Its weight rises quickly, peaking at 12% at about 80% RH, and then doubles to 25% beyond 80% RH, reflecting a highly porous internal structure capable of swift moisture adaptation. LLC5, composed of oleic acid liquid lipid and OraRez, exhibits significant weight fluctuations with sorption and desorption being asymmetric, peaking up to 42% at similar RH levels. This high sorption capacity is due to its liquid lipid composition, primarily oleic acid, allowing for substantial moisture interactions. The pronounced fluctuations during the desorption phase suggest an irregular pore distribution within LLC5, leading to differential rates of moisture absorption

and release. Therefore, the differences in moisture interaction among the formulations are influenced by both the types of lipids and the stabilizers used, highlighting the complex interplay between these components in determining the overall moisture sorption characteristics.

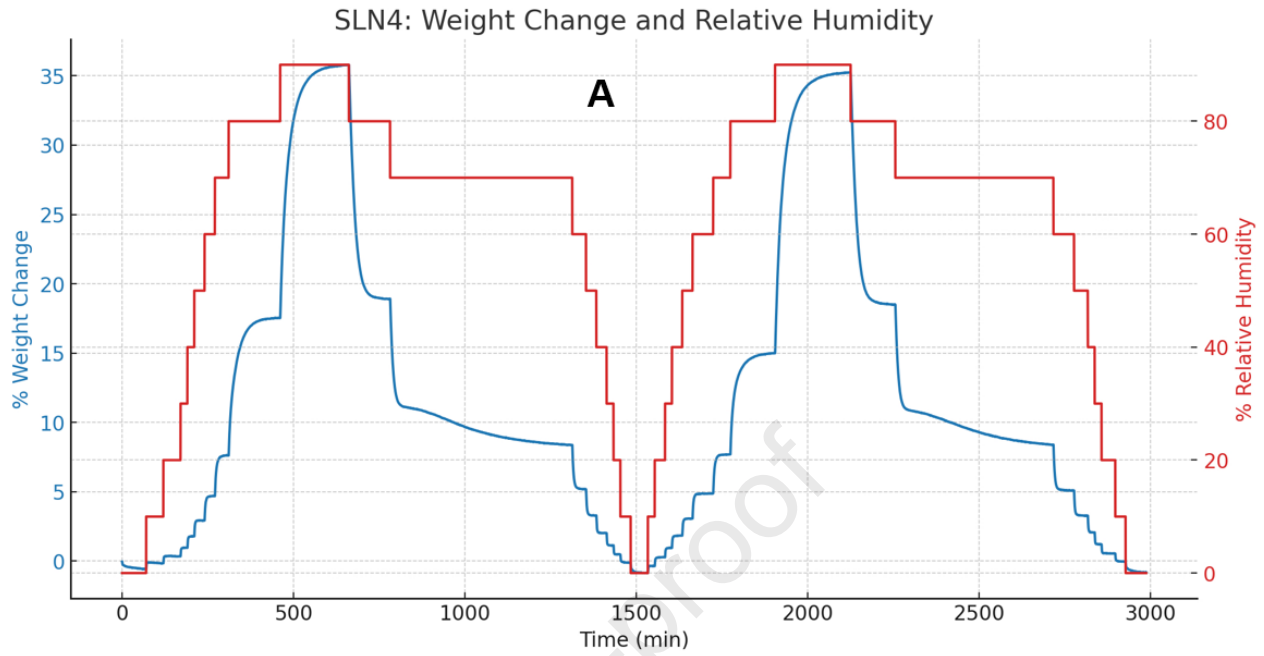

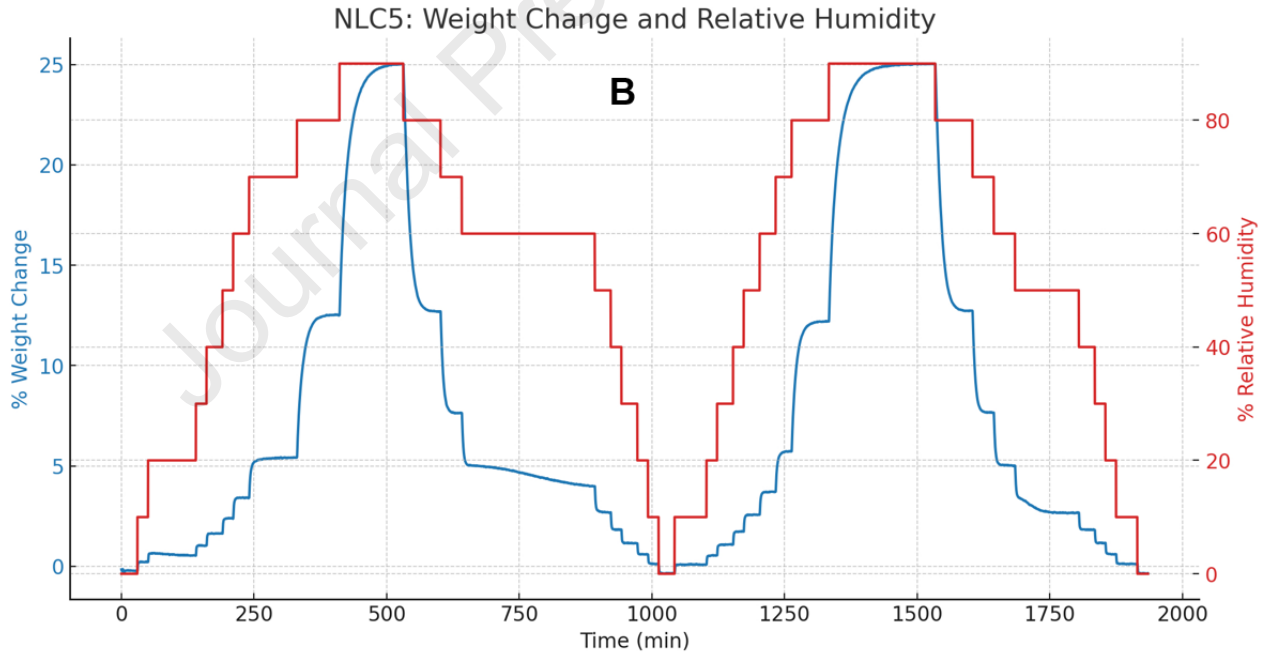

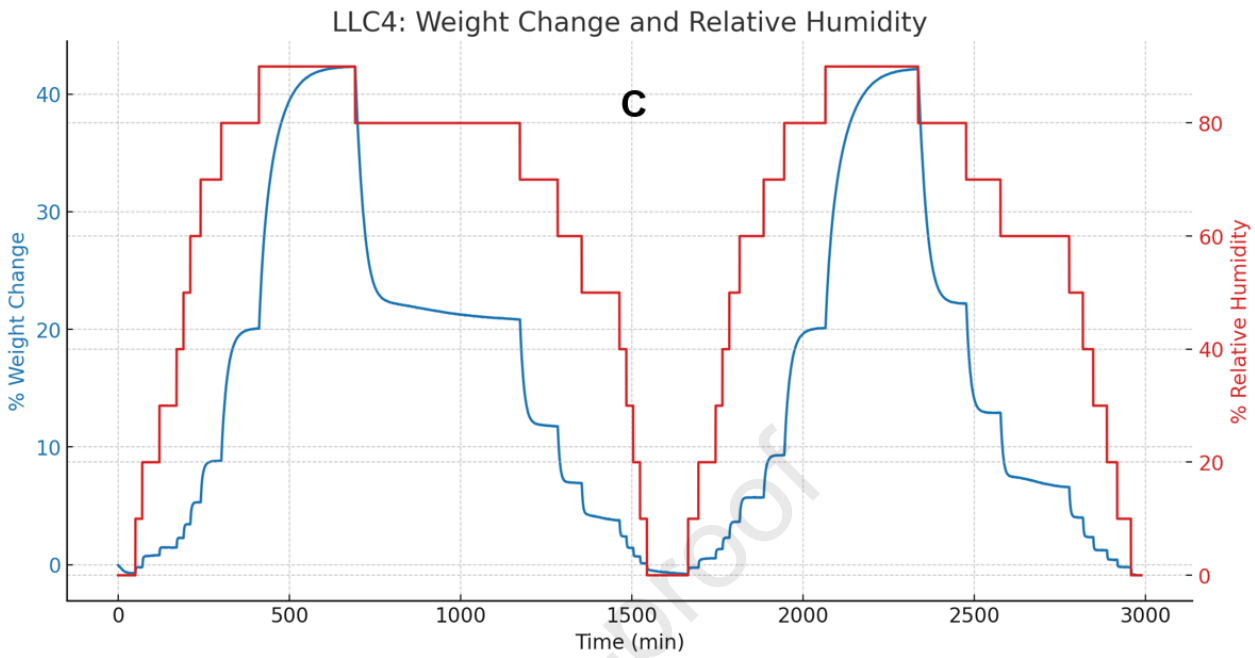

Figure 5. Dynamic Vapor Sorption profiles of various spray-dried LNP formulations, displaying characteristic moisture uptake and release over time for **(A)** SLN4**, (B)** NLC5, and **(C)** LLC4**.** The blue lines represent the weight change percentage, and the red lines indicate the relative humidity percentage over time.

3.4 Fourier Transform Infrared Spectroscopy (FTIR)

The FTIR spectroscopic analysis was performed to identify changes in chemical bonds and verify the encapsulation of PMZ within the spray-dried LNP formulations, revealing characteristic peaks for each compound. For PMZ, sharp peaks at 1697 cm^{-1} indicated C=O stretching, and bands between 1200 and 800 cm^{-1} suggested aromatic ring vibrations, characteristic of the PMZ fingerprint region [36]. Stearic acid's spectrum displayed a carbonyl stretch at about 1695 cm^{-1} and peaks at 2915 cm^{-1} and 2848 cm^{-1} due to aliphatic C-H stretching, representing methylene groups [37]. Oleic acid exhibited a strong carbonyl stretch near 1705 cm^{-1} and aliphatic C-H stretches in the 2850-2950 cm^{-1} range [38]. HPMC-E5 showed a peak at 1052 cm^{-1}, signifying C-O stretching of methoxy groups [39].

In **Figures 6 (A, B, and C)**, all spray-dried SLN, NLC, and LLC formulations demonstrated broadening of bands above 3000 cm^{-1}, suggesting hydrogen bond formation between

PMZ and lipid constituents. Specifically, **Figure 6 (A)** revealed significant changes in PMZ's aromatic C=C stretch at 1480 cm^{-1} and the C-H bending frequencies between 1225-1370 cm^{-1} in SLNs, displaying pronounced broadening and decreased peak intensities. The carbonyl group's C=O stretch at 1697 cm^{-1} also broadened. Stearic acid's characteristic carbonyl stretch shifted from 1690 cm^{-1} to 1700 cm^{-1} in SLNs, showing a decrease in intensity and more diffuse aliphatic C-H stretches. Methylene group vibrations also broadened, indicating potential crystallization or hydrogen bonding effects. In HPMC-E5 within SLN formulations, a shift in the C-O stretching vibration at 1052 cm^{-1} suggested a disruption in the molecular environment due to hydrogen bonding, further indicated by changes in the C=O stretching environment in **Figure 6 (A)** [40]. This was observed across SLN4, SLN5, and SLN6, pointing to modifications in the electronic environment around PMZ, consistent with an amorphization process and suggesting successful encapsulation by the lipid matrix.

Figure 6 (B) displayed subtle modifications in the carbonyl (C=O) group around 1700 cm-1 and the aromatic C-H bonds at 2958 cm-1 in NLC formulations, indicating changes due to drug interactions with lipid components or reorganization within the NLC structure.
Likewise, **Figure 6 (C)** highlighted changes in LLC formulations, with variations in the intensity and position of the C=O stretching vibration around 1700 cm^{-1} and minor shifts in the aromatic C-C stretching area around 1585 cm^{-1}, suggesting interaction between PMZ molecules and the lipid or polymer matrix, impacting the compound's stability and bioavailability. The interaction between PMZ molecules and the lipid or polymer matrix can significantly enhance the compound's stability by improving its oxidative and hydrolytic stability. Lipid matrices can shield PMZ from oxidative degradation, thereby extending its shelf life and maintaining therapeutic efficacy, while polymers act as barriers against moisture, reducing the risk of hydrolysis and preserving the compound's integrity in aqueous environments. Additionally, the bioavailability of PMZ is enhanced through improved solubility and controlled release mechanisms provided by the lipid or polymer matrices. These matrices can increase the solubility of PMZ, making it more readily available for absorption in biological systems. Moreover, they can enable a sustained release of PMZ, maintaining steady plasma levels and prolonging therapeutic effects, thus preventing possible toxicity associated with conventional dosing.

A

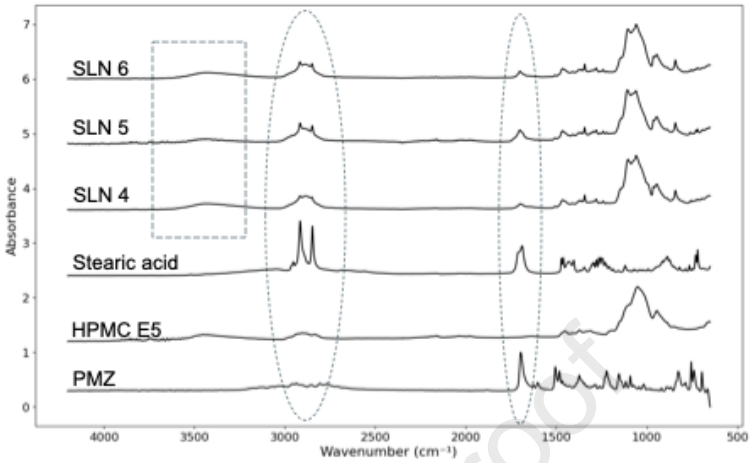

B

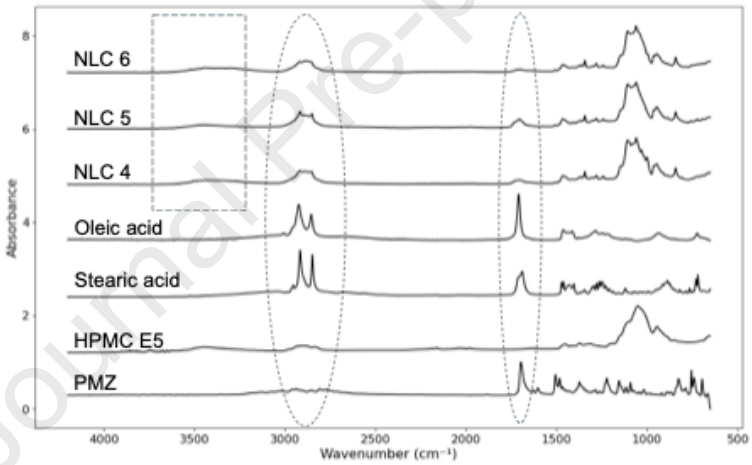

C

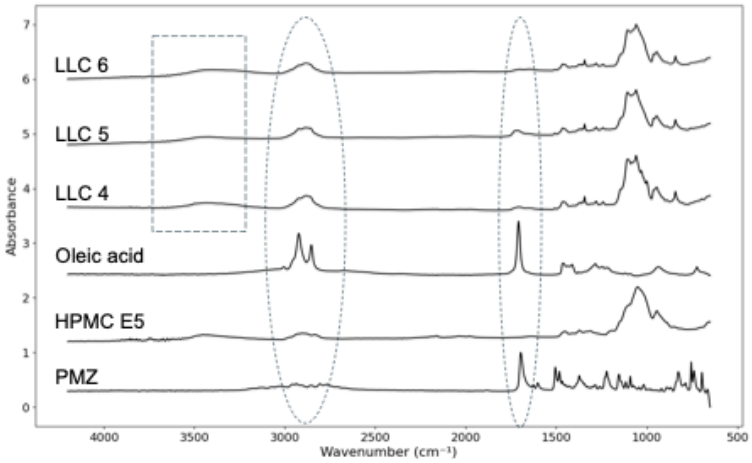

Figure 6. Fourier-transform infrared spectroscopy (FTIR) for (**A**) SLN4, **(B)** NLC, and (**C**) LLC formulations along with the pure components.

3.5 Raman spectroscopic analysis

Figure 7 shows different spectra of components used to prepare the formulations. The aim was to use each as a reference to map the surface of the formed particles using Raman confocal microscopy. This analysis provides insight on how different components are distributed and how can they affect dissolution and stability.

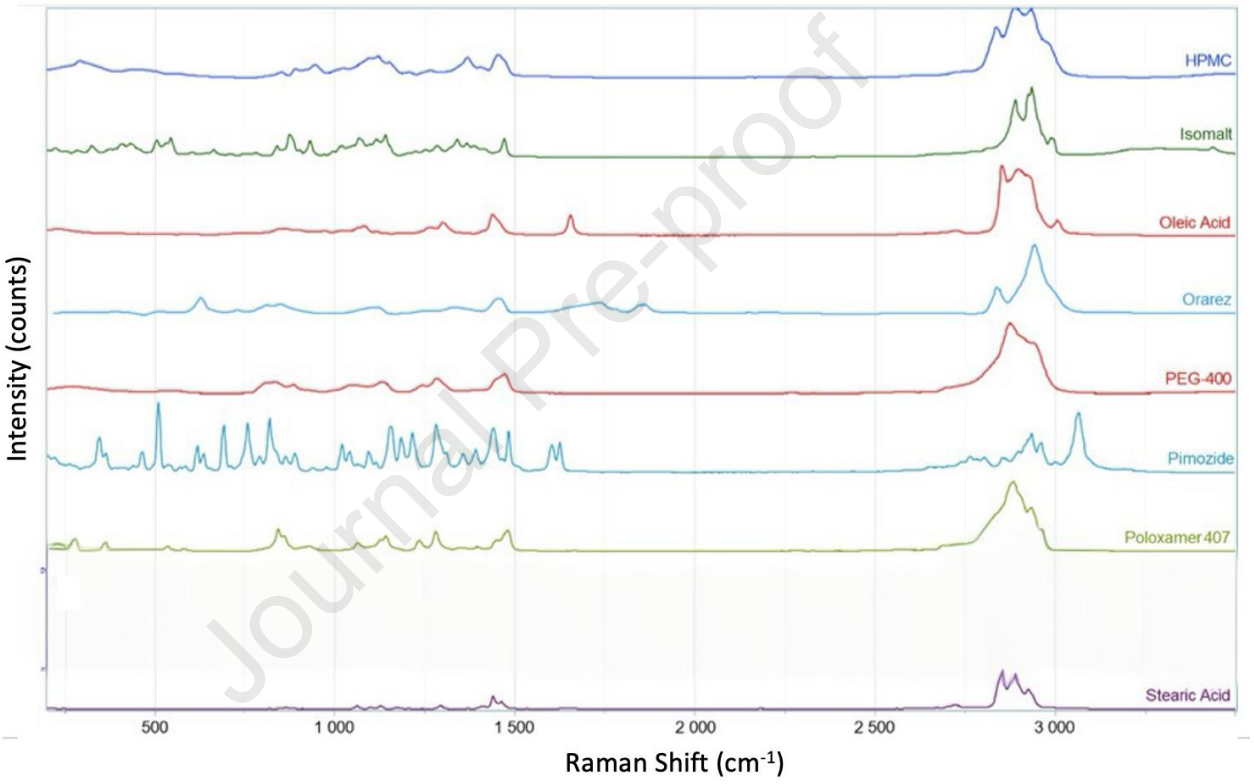

Figure 7. Raman spectra for the various components of spray-dried LNPs.

Figure 8 presents Raman maps showing the spatial distribution of stearic acid (A) and poloxamer 407 (B) within a selected region of the NLC sample. The bright areas in each map indicate regions with higher concentrations of the respective compounds, identified through their characteristic Raman signals. Notably, the two components appear predominantly co-located, suggesting potential interaction or structural association within the matrix. In contrast, no Raman signals corresponding to pimozide, oleic acid, PEG-400, or OraRez were detected in the mapped area, indicating these components are likely

not present on the surface. The ViewSharp™ white light image (C) at the bottom right provides a full-focus visual reference of the same region, allowing correlation between the chemical distribution and the sample's surface morphology.

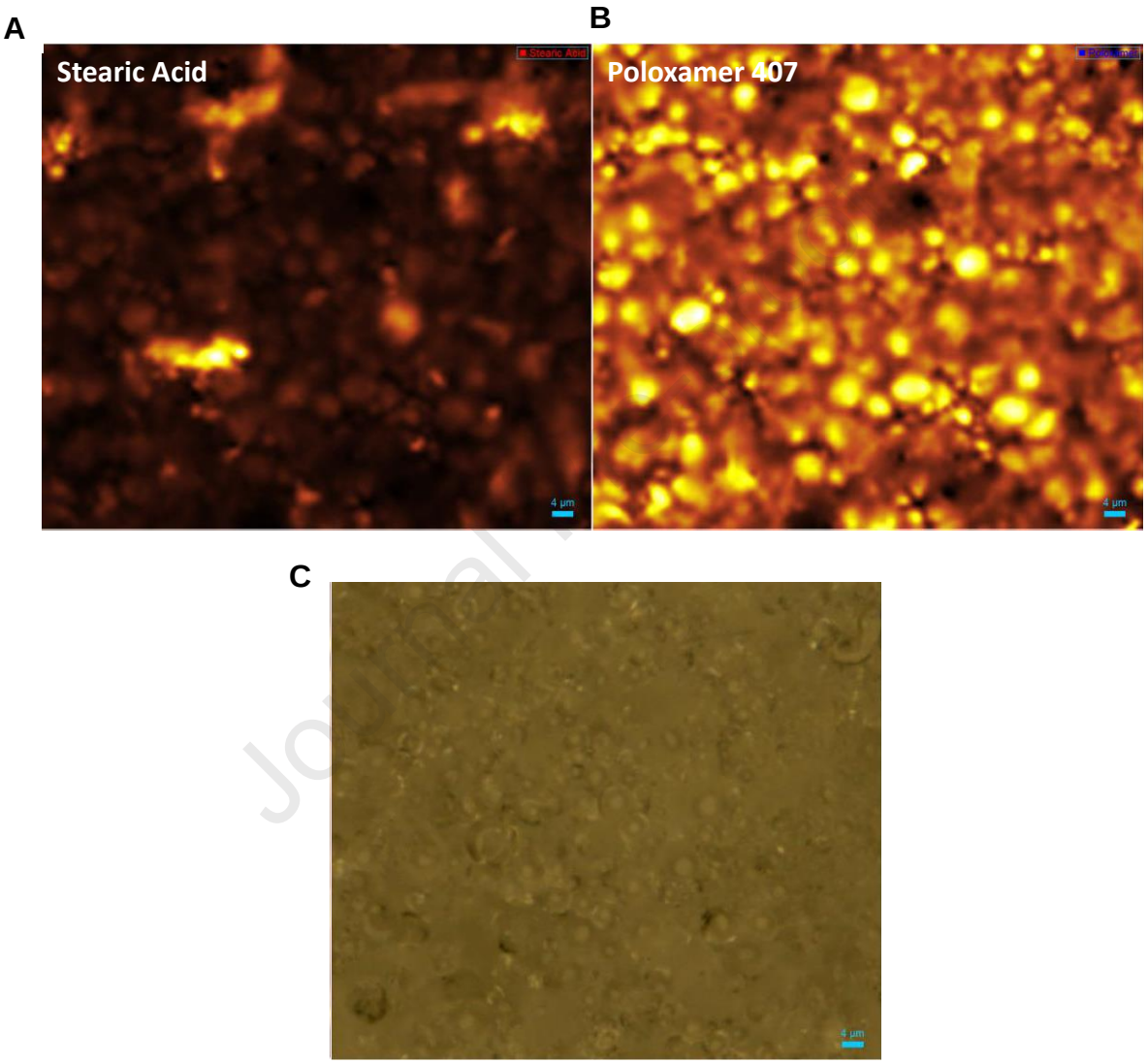

Figure 8. Raman maps illustrating the distribution of stearic acid and poloxamer 407 within the sample. (A) shows the spatial distribution of stearic acid, highlighted by its characteristic Raman signal. (B) displays the distribution of poloxamer 407, similarly identified by its distinct Raman signature. The bright areas in both Raman maps indicate regions with a higher concentration of the respective substances. (C) is a full-focus white light image of the same sample region, providing a visual reference for the overall

morphology and aiding in correlating the Raman mapping data with the physical structure of the sample. Scale bars represent 4 µm.

To form an overall impression of the chemical distribution of the NLC sample, a false colour map (combining all constituents (each constituent is allocated a colour) has been generated **(Figure 9)**. The majority of the grains show as cyan indicating again that the poloxamer (green) and the polymer (blue) are co-located. Individual grains of stearic acid (red) are clearly visible.

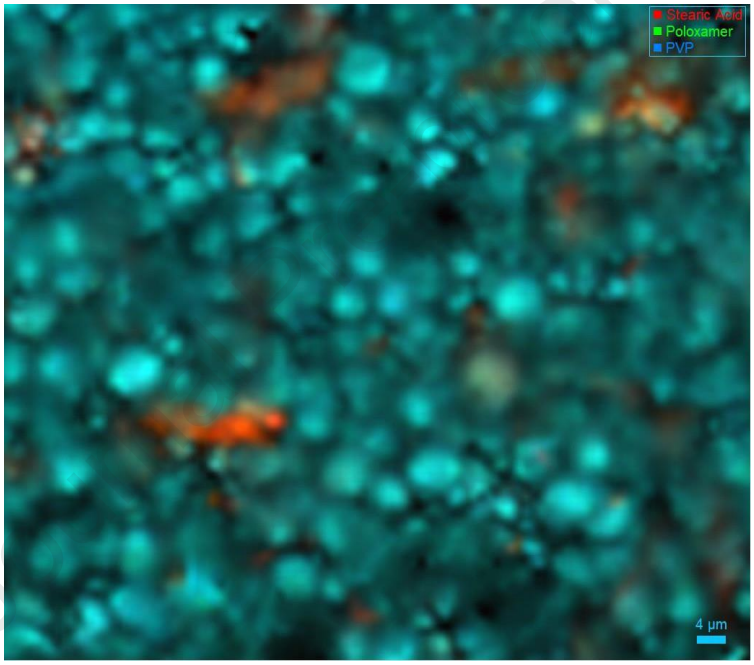

Figure 9. Chemical map illustrating the distribution of constituents in a spray-dried nanostructured lipid carrier (NLC) sample. The map is colour-coded to show the spatial distribution of different components: poloxamer (green) and polymer (blue) are co-located, resulting in most grains appearing cyan. Individual grains of stearic acid (red) are clearly visible, indicating areas where this constituent is concentrated. The scale bar represents 4 µm, providing a reference for the size of the particles.

A comparison was made with an LLC sample to understand the impact of excluding the solid lipid (stearic acid) as can be seen in **Figure 10**. Individual maps of the locations of the various constituents are shown. The individual grains can be clearly seen. There is evidence that the oleic acid and PEG-400 are co located.

A

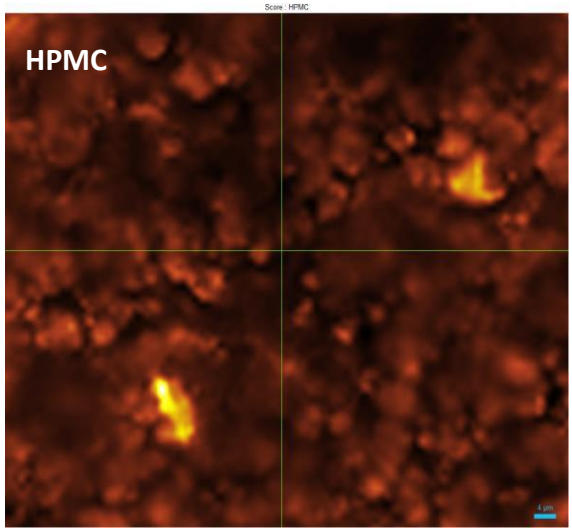

B

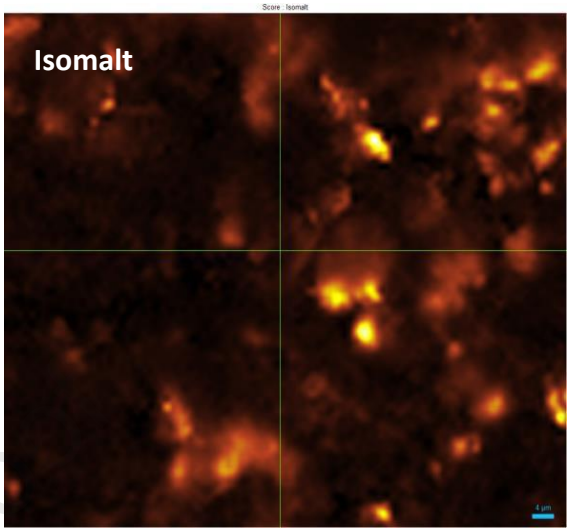

C

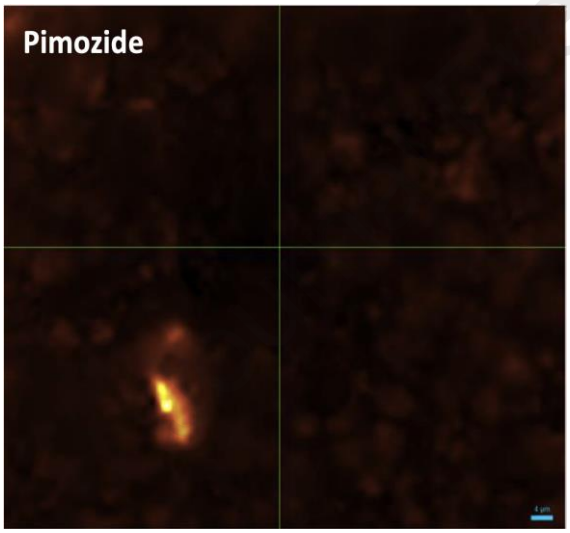

D

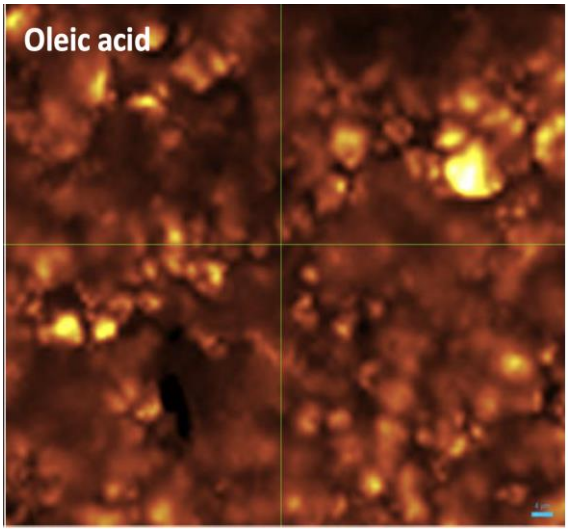

E

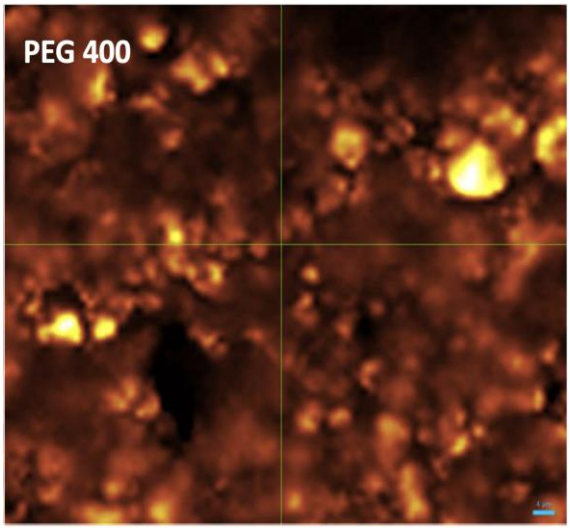

F

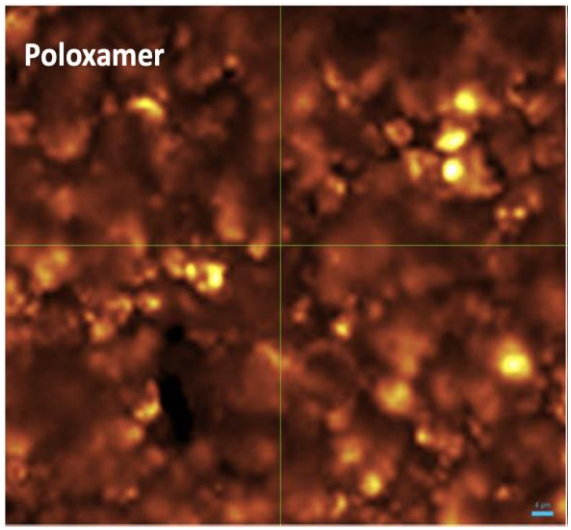

Figure 10. False colour maps illustrating the spatial distribution of various constituents in a spray-dried lipid liquid crystalline (LLC) sample. The images show the distribution of HPMC (A), isomalt (B), pimozide (C), oleic acid (D), PEG 400 (E), and poloxamer 407 (F). Each map highlights the specific location and concentration of these components within the sample. Bright areas in each map represent regions with a higher concentration of the respective constituent. The scale bar in each image represents 4 µm, providing a reference for the size of the observed features. These maps help visualize the co-localization and distribution patterns of the different compounds within the spray-dried matrix.

To visualize the overall chemical distribution within the spray-dried LLC sample, a false colour map (combining all constituents (each constituent is allocated a colour) was generated as shown in **Figure 11A**. Additionally, **Figure 11B** represents an overlay the of the pimozide signal (green) onto the corresponding white light image, allowing a direct visual comparison between the chemical and morphological data. The power of Raman spectroscopy is highlighted by the lack of obvious correlation with the white light image. The white light image cannot be used alone to identify the location of the drug particles.

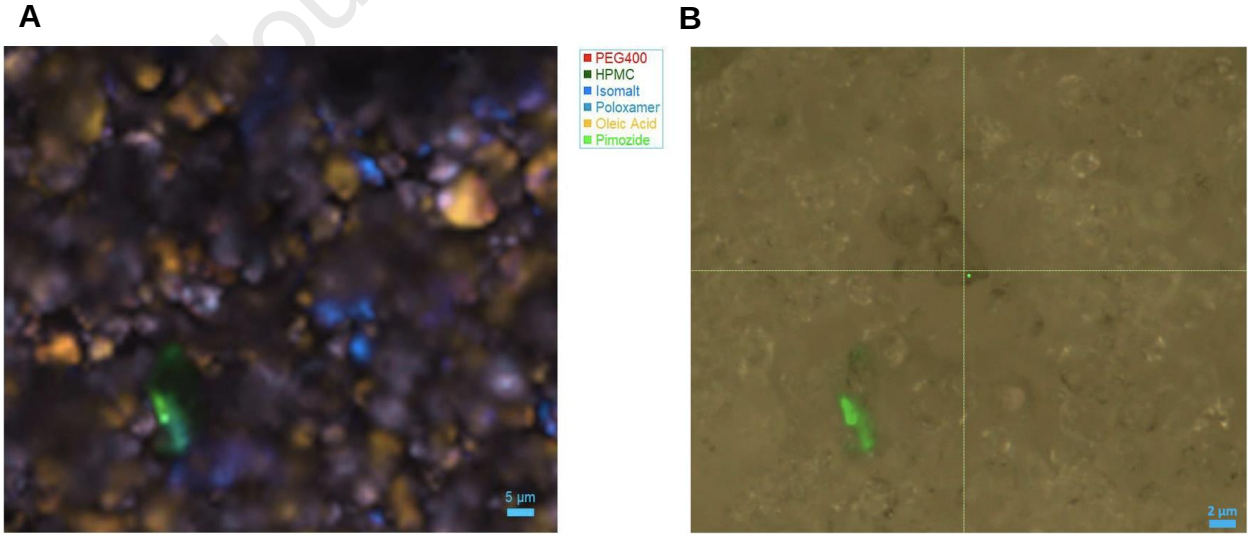

Figure 11. False colour chemical map (A) and overlay (B) illustrating the distribution of various constituents within a spray-dried lipid liquid crystalline (LLC) sample. (A) presents a false colour map where different colours represent distinct constituents: PEG 400 (red), HPMC (purple), isomalt (blue), poloxamer (cyan), oleic acid (yellow), and pimozide (green). This map visualizes the spatial distribution and co-localization of these components within the sample. (B) shows an overlay of the location of pimozide (green) relative to the white light image of the same region, providing a visual correlation between the chemical map and the sample's physical structure.

Overall, the distribution of all the constituents was clearly observed. The silicon measurement showed that the background in the zoomed region is due to photoluminescence within the silicon, not a measurement artefact. To avoid any confusion, the data presented has not been baselined, smoothed, or subjected to any other form of data processing.

In this study, Raman spectroscopy was utilized to analyze both the structural and chemical properties of spray-dried LNPs, focusing on how oleic acid disrupts the lipid matrix to enhance EE%, supported by XRPD results documented in Section 3.6. This technique generated detailed false-color chemical maps that depicted the spatial co-localization of oleic acid and PEG-400, crucial for boosting drug loading capabilities. Furthermore, Raman maps pinpointed the presence of poloxamer 407, HPMC, and pimozide, demonstrating the method's exceptional capacity to reveal molecular arrangements not visible through traditional white light imaging.

Additionally, consistent with the changes noted in the FTIR analysis from Section 3.4, which showed interactions between the drug PMZ and various components of the lipid or polymer matrix, Raman spectroscopy provided detailed chemical maps. These maps clearly displayed how oleic acid and PEG-400 are co-located. The maps, using false-colours, outlined how PMZ, oleic acid, poloxamer 407, PEG-400, HPMC, and isomalt are distributed. They confirmed the presence of PMZ and all other ingredients in the spray-dried LNP sample, demonstrating that oleic acid was deliberately added to modify the lipid matrix, thus enhancing the drug's loading capacity and stability.

Moreover, the Raman maps for the NLC sample showed substantial co-localization of poloxamer and the polymer, suggesting possible molecular interactions that were not detectable on the surface, as evidenced by the absence of PMZ, oleic acid, PEG-400, and OraRez in specific areas. The analysis of the LLC sample further reinforced the concept of increased molecular interactions within the more amorphous structures, as indicated by the XRPD data, through the observed co-location of oleic acid and PEG-400.

3.6 X-ray powder diffraction (XRPD)

XRPD analysis were conducted to assess how various components, affect the structural arrangement of nine spray-dried lipid nano formulations. The diffraction patterns of these formulations, which utilized stearic and oleic acids as solid and liquid lipids, respectively, are displayed in **Figure 12**. The analysis of pimozide's crystalline structure, as revealed through X-ray diffraction patterns, highlighted several prominent peaks that underscore its distinct molecular arrangement. Notably, a prominent peak at 2-theta value around 5˚ exhibited an intensity of 196. Additional peaks of equal intensity 187 were observed at 2-theta positions ranging between, 5˚ and 6˚. Furthermore, the analysis identified other important peaks located at 2-theta values of 16˚, 17˚, 19˚, and 20˚. In the diffraction patterns of stearic acid, major peaks at 2-theta values of around 6˚ and 10˚ were identified as characteristic of stearic acid.

Additionally, the observation of two peaks at 2-theta values of 19˚ and 23˚ suggested the presence of poloxamer 407, possibly located on the surface of all SLN, NLC, and LLC samples. The XRPD patterns presented in **Figure 12** revealed varying degrees of amorphization across the different spray-dried LNPs, with the order being LLC>NLC>SLN in terms of amorphous content. SLNs had sharper, more intense peaks, indicating increased crystallinity due to enhanced molecular ordering within the lipid matrix [41]. **Figure 12 (A)** revealed the highest degree of crystallinity in the structures of SLN formulations. Where they kept the crystal pattern of PMZ and poloxamer- 407, with many peaks, showing that PMZ's crystal structure was mostly present within the spray-dried SLN samples.

NLCs displayed a trend towards more amorphous structures, possibly as a result of the mixed lipid matrix interfering with crystal lattice and causing structural defects from nano-sizing, and crucial lipid matrix interactions [42]. **Figure 12 (B)** showed that NLC formulations appeared to undergo more significant transformations, potentially leading to a mix of crystalline and amorphous structures. In contrast, the LLC nanoparticles exhibited decrease in peak intensity and a pronounced shift towards amorphous structures, attributed to a more disrupted lipid matrix, potentially due to the sole use of oleic acid.

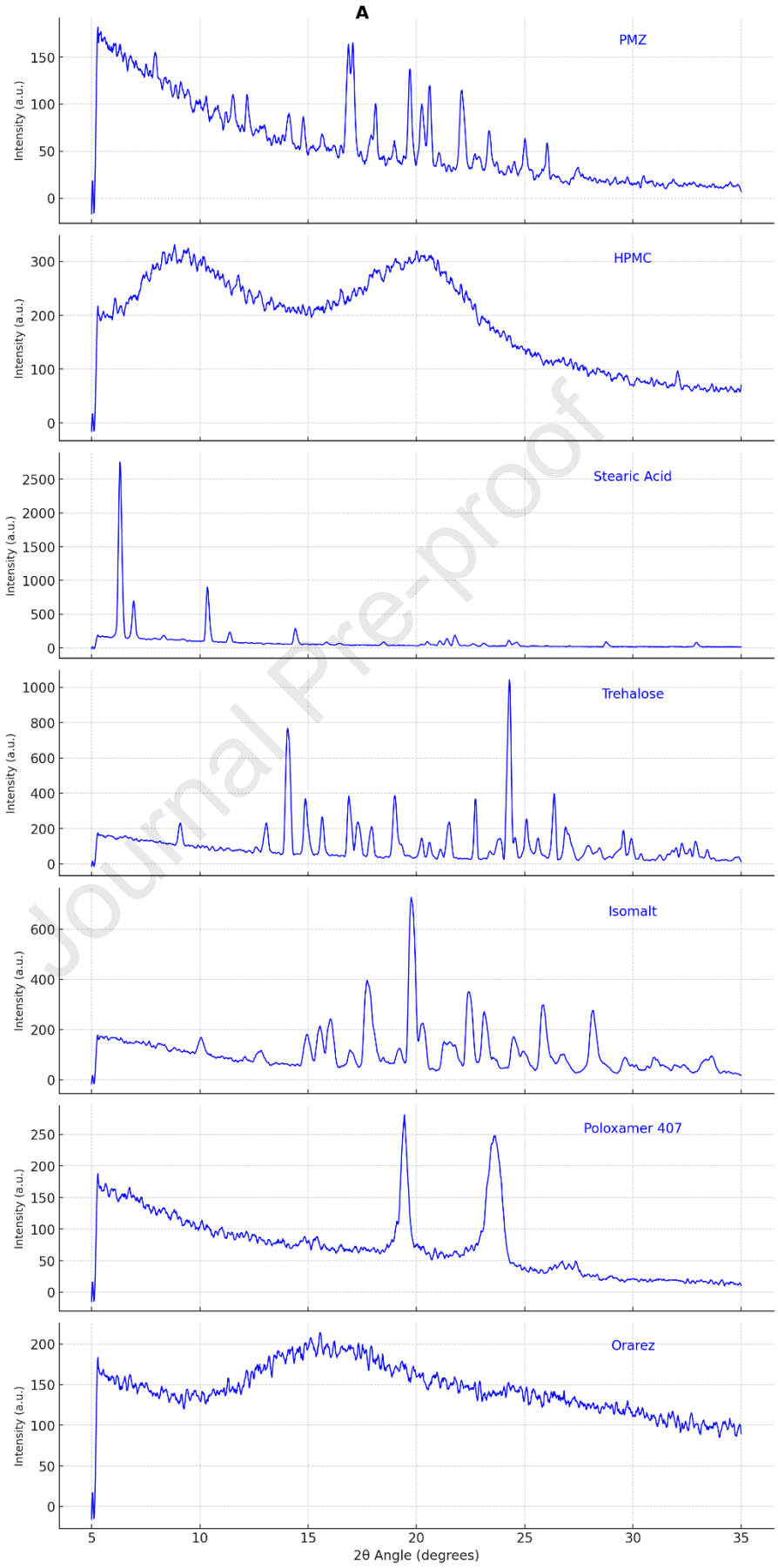

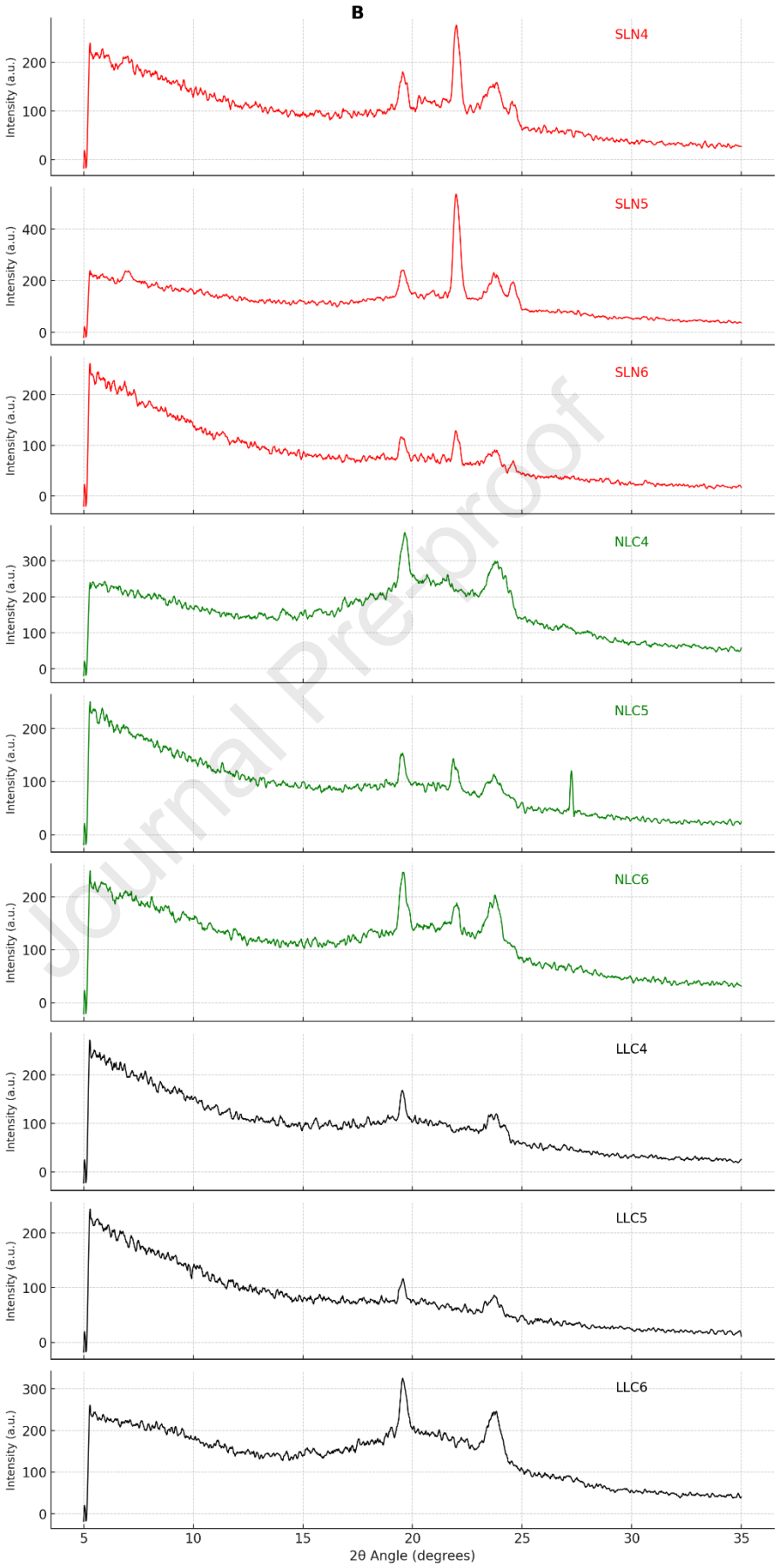

Figure 12. X-ray powder diffraction (XRPD) patterns of **(A)** pimozide (PMZ), HPMC-E5, stearic acid, trehalose, isomalt, and poloxamer 407, OraRez and **(B)** Spray-dried LNPs, including Solid lipid nanoparticles (SLNs) in red, Nanostructured lipid carriers (NLCs) in green, Liquid lipid carriers (LLCs) in black.

3.7 Surface morphology

A key finding from the SEM images, as depicted in **Figure 13 (A, B, and C)**, is that each formulation experienced size growth after spray drying, transforming from nanoparticles to microparticles. This increase in size might have resulted from the nanoparticles aggregating or fusion during the spray drying process [22, 25].

SEM images of SLN4 showed a mix of spherical particles and large lipid aggregates, while NLC5 displayed clusters that could be attributed to either shrinkage from drying or the concentration of the dispersion medium. **Figure 13 (A)** showed nanoparticles with a predominantly rounded morphology and a relatively smooth surface, with minor wrinkles and indentations [43, 44]. Notably, the smoother surface texture of SLN4, compared to NLC5 and LLC4, along with the presence of micro-wrinkles, could diminish particle cohesion, thus improving dispersibility. The incorporation of trehalose in SLN4 is believed to provide a glassy surface to the particles, further reducing stickiness and enhancing flowability [45].

NLC5 particles in **Figure 13 (B**) were distinguished by a mix of large, flake-like structures and smaller, rounded particles with irregular sizes and collapsed sides, a characteristic of spray-dried particles. Such variations in shape are suggested to result from the interaction dynamics between stearic and oleic acids during spray-drying. The surface roughness observed in NLC5 could potentially lower effective density and improve air suspension, crucial for consistent dose delivery.

SEM images of LLC4 in **Figure 13 (C)** revealed a non-spherical shape with a wrinkled, rough texture. The rough surface could reduce particle cohesion, essential for preventing aggregation and ensuring uniform particle dispersion during aerosolization and deep lung delivery [46]. The aggregation tendency observed could impact aerosolization efficiency

and respiratory tract deposition. However, the inclusion of trehalose was expected to stabilize the particles and aid in de-aggregation upon inhalation, enhancing dispersibility and deep lung penetration [45].

The observed morphologies in the SEM images can be attributed to the lipid composition, stabilizers, and the spray-drying process. For SLN4, the solid lipid crystallizes upon cooling, forming a relatively uniform and crystalline structure, with trehalose acting as a stabilizer that provides a glassy surface, reducing stickiness and enhancing flowability. In NLC5, the combination of solid and liquid lipids disrupts the crystalline lattice, leading to heterogeneous and less ordered structures with phase separation features. The OraRez stabilizer contributes to surface roughness, which can lower effective density and improve air suspension. For LLC4, the exclusive use of liquid lipids results in a highly irregular and amorphous structure due to the absence of crystallization, with trehalose helping to stabilize the particles and prevent aggregation. These variations in lipid composition and the role of stabilizers during the spray-drying process are key to understanding the distinct particle morphologies observed in the SEM images.

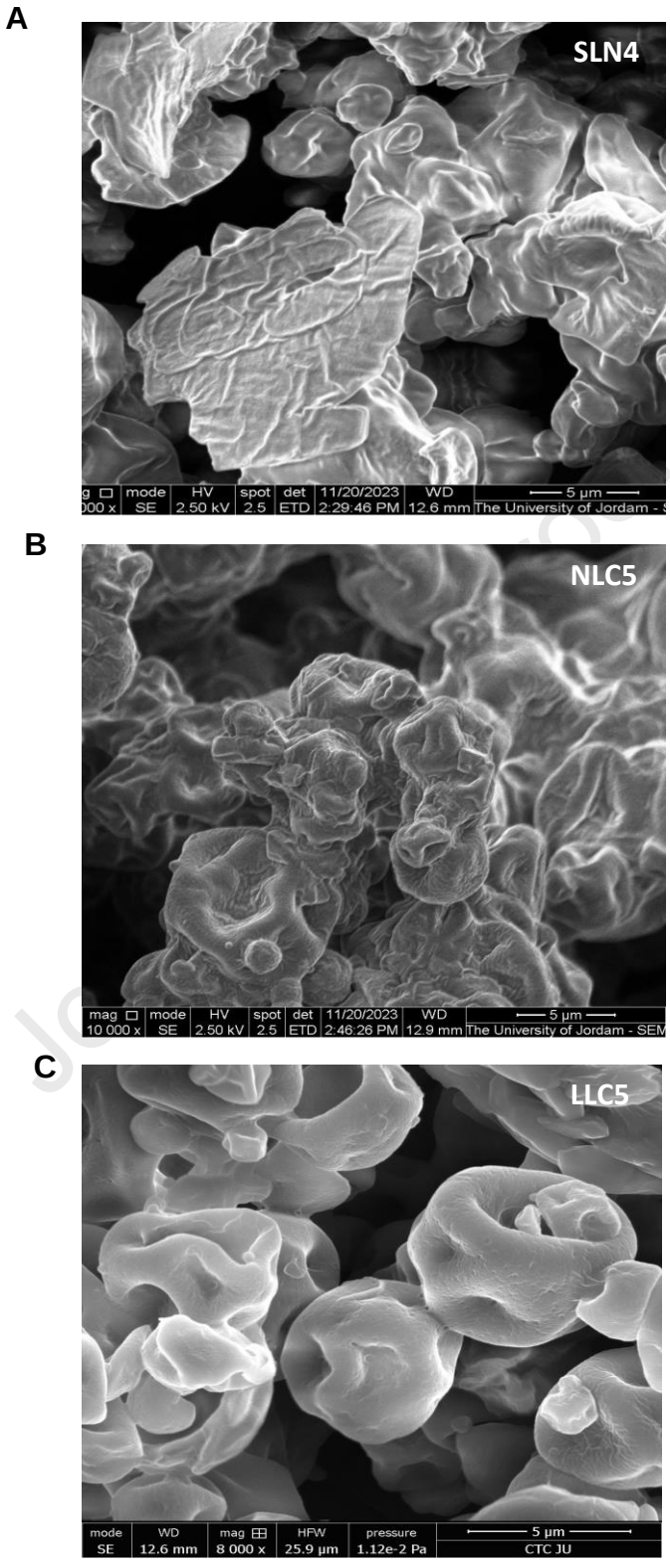

Figure 13. SEM images of SLN4 (A), NLC5 (B), and LLC4 (C) spray-dried LNPs

3.8 Evaluating the anti-proliferative activity of pimozide loaded lipid nanoparticles against A549 cells

After conducting experiments, on nanoparticles containing PMZ and observing their impact on halting the growth of lung cancer cells, we utilized the MTT assay to assess their ability to inhibit cell proliferation. NLC 4 NLC 5 and LLC 5 emerged as promising candidates among the tested formulations due to their effectiveness in impacting cell growth. The results of the MTT assay indicated that these spray dried LNP formulations were more successful than PMZ in impeding cell line growth. Specifically, NLC 4 showed an IC50 value of 8.00 μM (±0.94 μM) NLC 5 had a value of 7.52 μM (±1.20 μM). LLC 5 had a value of 9.39 μM (±1.16 μM) compared to PMZs IC50 value of 13.27 μM (±0.41 μM) as illustrated in **Figure 14A**. These results align with studies conducted by Li et al. (2020) Wiklund et al. (2010). Dakir et al. (2018) that reported IC50 values, for PMZ [3, 47, 48].

To verify that the slowdown, in cell growth caused by the formulations stemmed from PMZ alone and not from the components we examined how the excipients impacted cell growth. As shown in **Figure 14B**, the experiments revealed that at a concentration of 1 mg/mL the excipients did not hinder the growth of cells in a lab setting. This observation backs the notion that it's indeed the PMZ content, rather than the excipients that is responsible, for the anti-proliferative effect of the formulation.

Statistical analysis of IC50 values indicated that the difference between the spray-dried LNP formulations and free PMZ was statistically significant as elucidated in **Figure 15**.

The superior anti-proliferative performance of PMZ when formulated into nanoparticles as opposed to its free form could be attributed to improved cellular penetration and solubility [49]. The challenge of poor water solubility and limited bioavailability, common to many anticancer drugs including PMZ, often negatively impact their therapeutic efficacy [50]. The strategy of nanoparticle encapsulation not only seeks to increase solubility but also to enhance the drug's anti-proliferative effect.

An example of such enhancement in solubility and bioavailability through nanoparticle technology is Doxil®, a liposomal formulation of doxorubicin, which ensures effective drug delivery to tumor sites while reducing cardiotoxicity [51]. Furthermore, nanoparticles may increase the penetration of drugs into cancer cells, facilitating the release of the encapsulated drug to intracellular targets and thus enhancing its therapeutic effect. This

concept is supported by findings from Swidan et al. (2016), who noted an increase in tumor cell penetration and cytotoxicity of paclitaxel when formulated into NLC [29]. However, these attributes need to be further investigated.

A

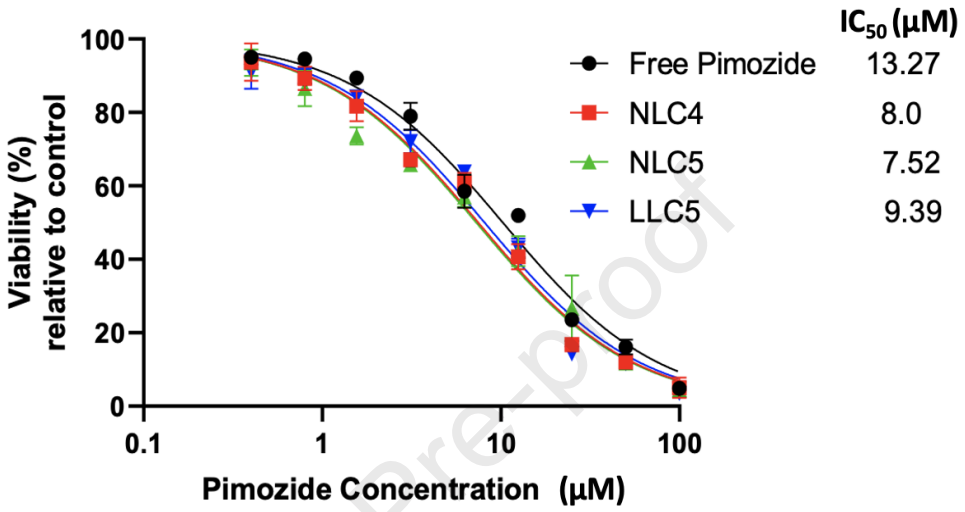

B

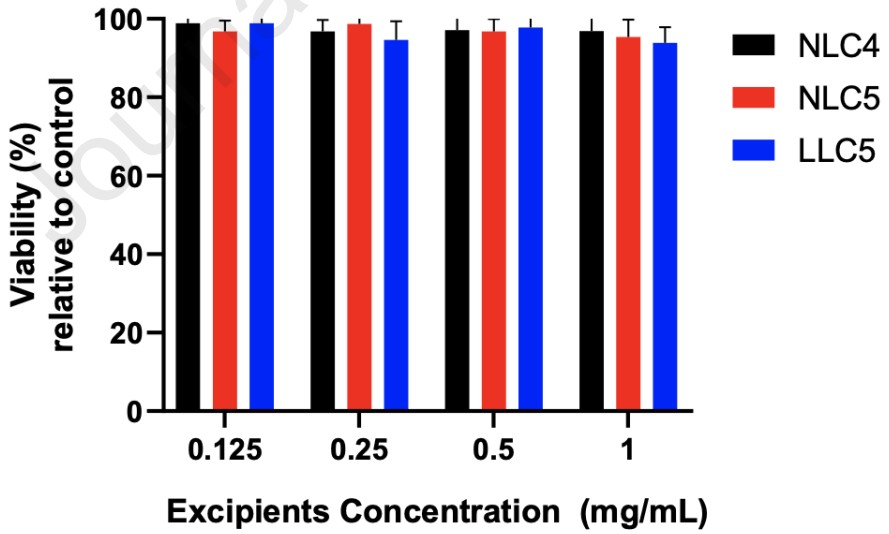

Figure 14. Anti-proliferative effect of free pimozide, and its spray-dried lipid nano formulations NLC4, NLC5, and LLC5 **(A)** and blank excipients **(B)** against A549 cell line mode following 72 hours of treatment. Graphs are presented as percentage viability relative to the untreated control. Data represent the mean ± S.D.

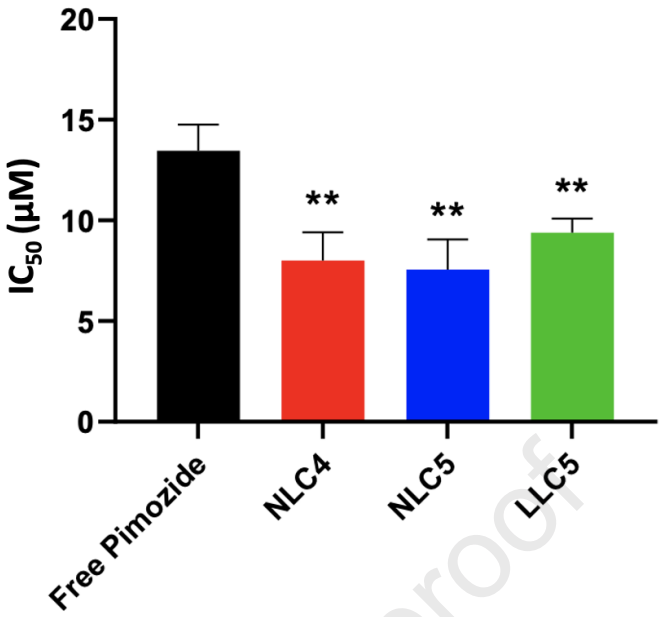

Figure 15. Bar graph showing the IC_{50} values for four different groups: Free pimozide, NLC 4, NLC 5, and LLC 5. ** $p < 0.01$ was calculated using one-way ANOVA. Data presented as mean ± SD.

3.9 Drug release studies

Following the identification of the promising anti-proliferative capabilities of NLC4, NLC5, and LLC5, their drug release profiles were carefully evaluated to determine how PMZ is delivered over time. Additionally, the release kinetic of free pimozide was evaluated. In the evaluation of the PMZ release profile from the formulations, a biphasic release pattern was observed followed by a sustained release phase. The release of PMZ as illustrated in **Figure 16** followed a biphasic manner with a mean of 18.9% ±2.07% after 2 hours. The release rate then reached 51.8% ±4.21% by 8 hours. This phase continued over the 72-hour period, peaking in a mean release of 89.2% ±3.08.

Similarly, PMZ release from NLC5 was biphasic, with a little lower first burst, yielding a mean release of 17.1% ±2.51% at 2 hours. At 72 hours, this formulation had a slightly greater mean release of 92.0% ±2.61%, indicating a more consistent sustained phase. LLC5 had the slowest initial burst among the three formulations, exhibiting a biphasic PMZ release pattern with a mean release of 15.9% ±3.28% after 2 hours. The chemical was

consistently released over the trial duration, reaching a mean of 89.8% ±2.37% by 72 hours, comparable to NLC4.

Free pimozide showed a markedly higher release 62.5 ± 2.50% compared to the lipid-based nanoparticles at the 2-hour mark. This trend of free pimozide leading the release continued at the 4-hour time point, reaching 94.2 ± 3.48% indicating an almost complete release. The biphasic release pattern characterized by an initial rapid release followed by a more gradual, sustained phase, corroborating previous studies [52-54]. The initial burst of drug release is thought to arise from drug molecules that are loosely bound to the surfaces of the nanoparticles, allowing for their quick dissemination into the target area [54]. This dual-phase release mechanism of the formulations may offer considerable advantages for inhalation therapy in NSCLC treatment by ensuring prolonged drug presence in the lung tissue, which could lead to sustained anti-cancer effects [55]. This may enhance the overall therapeutic efficacy, allowing for reduced dosing frequencies, thereby improving patient which could significantly impact the clinical management of NSCLC, potentially enhancing patient outcomes.

The initial burst release is primarily driven by the presence of free or loosely bound drug on the surface of the nanoparticles. This unencapsulated drug is readily available for dissolution and diffusion upon exposure to the release medium. In this study, free pimozide exhibits a rapid release, with approximately 60-64% of the drug released within the first two hours, reaching up to 98% by eight hours. This significant initial burst suggests that a considerable portion of the drug is present either as a free drug or is poorly encapsulated, residing near or on the surface of the nanoparticles. This phase represents the unencapsulated drug fraction, which is immediately available to dissolve and diffuse out.

Following the initial burst, the formulations enter a more controlled and sustained release phase. This phase is governed by the release of the drug encapsulated within the nanoparticle matrix. The release kinetics during this phase are typically controlled by diffusion through the nanoparticle material, degradation or erosion of the nanoparticle matrix, or a combination of both processes. For instance, LLC 5 continues to release up to 92% of the drug over 72 hours, while NLC 5 and NLC 4 demonstrate a gradual increase in release up to around 94% and 92%, respectively. This sustained release phase

indicates the controlled release of the drug from within the nanoparticle, where the matrix acts as a barrier to drug diffusion and degradation.

The nanoparticle phase plays a crucial role in determining the release kinetics of the encapsulated drug. In NLC and LLC formulations, the lipid composition whether solid, and liquid, or only liquid significantly affects the release behavior. Solid lipids generally provide a more rigid structure, which limits the diffusion of the encapsulated drug, thereby offering a slower and more controlled release. In contrast, liquid lipids may allow for faster diffusion, contributing to a more rapid release profile. The observed release characteristics of LLC 5, NLC 5, and NLC 4 suggest that these formulations likely contain a mixture of solid and liquid lipids, typical of NLCs, or possibly entirely liquid lipids for LLCs, which contributes to the observed release kinetics.

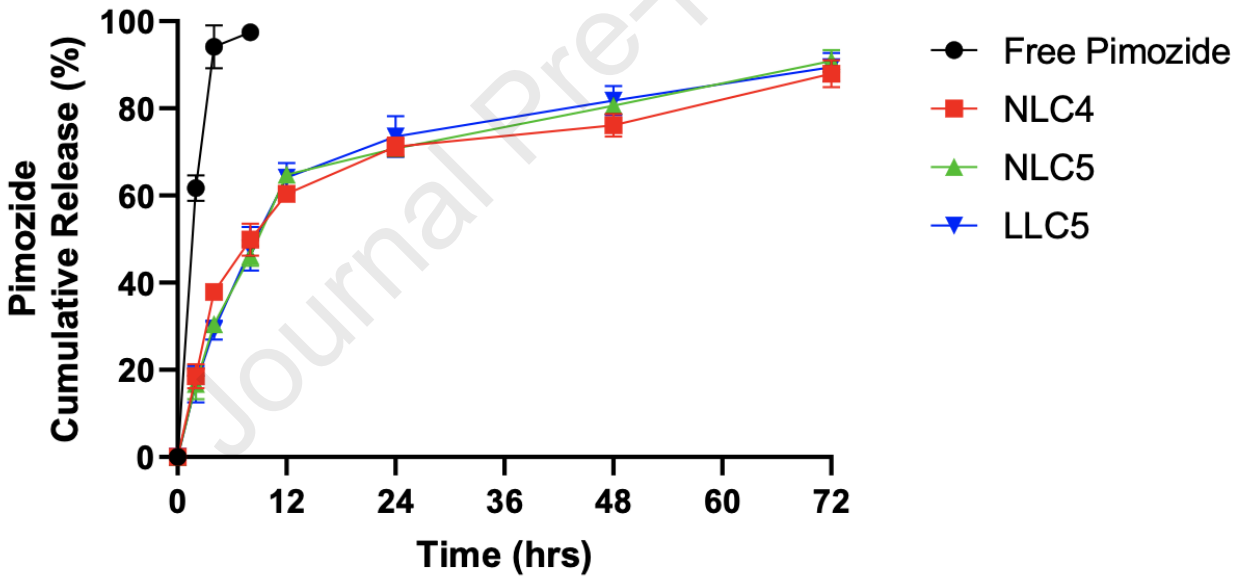

Figure 16. Time-dependent release kinetics of pimozide from three distinct spray-dried lipid formulations: NLC4, NLC5, and LLC5 compared to the free pimozide. Each panel represents the percentage of pimozide released over a 72-hour period, highlighting the biphasic release pattern characterized by an initial burst followed by a sustained release phase. Free drug were used as control; values are means ± SD.

4. Conclusions

This study demonstrates the potential of pimozide-loaded lipid nanoparticles (LNPs) as a transformative approach to the targeted treatment of NSCLC. By employing the microemulsion technique to develop and optimize SLN, NLC, and LLC formulations, the research advances drug delivery technology through precise control over particle properties, encapsulation efficiency, and drug release profiles. Notably, the incorporation of oleic acid into NLC formulations significantly enhanced encapsulation efficiency and drug stability, highlighting the versatility of lipid-based delivery systems in addressing the challenges of anticancer therapy.

The physicochemical analyses, including FTIR, Raman spectroscopy, and XRPD, provided a robust understanding of drug-lipid interactions, structural integrity, and the molecular dynamics of these formulations. The demonstrated anti-proliferative effects against A549 lung cancer cells, combined with sustained and controlled release, underscore the potential of these formulations as effective alternatives to conventional chemotherapy, offering the dual benefits of enhanced efficacy and reduced systemic toxicity.

Looking forward, this study lays the groundwork for future research exploring in vivo efficacy, pharmacokinetics, and safety, alongside an in-depth examination of the underlying mechanisms driving the therapeutic success of these formulations. Such investigations will be pivotal in bridging the gap between laboratory findings and clinical applications, paving the way for innovative and patient-centered treatment strategies in NSCLC.

Conflict of Interest Disclosure: The authors declare no conflict of interest.

Acknowledgment: The authors would like to thank the Chemical Analysis Facility (CAF) at the University of Reading for providing essential access to instruments used in this study.

Reference:

[1] N. Duma, R. Santana-Davila, and J. R. Molina, "Non–small cell lung cancer: epidemiology, screening, diagnosis, and treatment," in *Mayo Clinic Proceedings*, 2019, vol. 94, no. 8: Elsevier, pp. 1623-1640.

[2] S. Pushpakom *et al.*, "Drug repurposing: progress, challenges and recommendations," *Nature reviews Drug discovery,* vol. 18, no. 1, pp. 41-58, 2019.

[3] B. Li *et al.*, "A novel drug repurposing approach for non-small cell lung cancer using deep learning," *PLoS One,* vol. 15, no. 6, p. e0233112, 2020.

[4] N. Vlachos, M. Lampros, S. Voulgaris, and G. A. Alexiou, "Repurposing Antipsychotics for Cancer Treatment," (in eng), *Biomedicines,* vol. 9, no. 12, Nov 28 2021, doi: 10.3390/biomedicines9121785.

[5] P. Ghasemiyeh and S. Mohammadi-Samani, "Solid lipid nanoparticles and nanostructured lipid carriers as novel drug delivery systems: Applications, advantages and disadvantages," *Research in pharmaceutical sciences,* vol. 13, no. 4, pp. 288-303, 2018.

[6] X.-Y. Ying, Y.-Z. Du, W.-W. Chen, H. Yuan, and F.-Q. Hu, "Preparation and characterization of modified lipid nanoparticles for doxorubicin controlled release," *Die Pharmazie-An International Journal of Pharmaceutical Sciences,* vol. 63, no. 12, pp. 878-882, 2008.

[7] E. W. Leong and R. Ge, "Lipid nanoparticles as delivery vehicles for inhaled therapeutics," *Biomedicines,* vol. 10, no. 9, p. 2179, 2022.

[8] A. Saedi, K. Rostamizadeh, M. Parsa, N. Dalali, and N. Ahmadi, "Preparation and characterization of nanostructured lipid carriers as drug delivery system: Influence of liquid lipid types on loading and cytotoxicity," *Chemistry and physics of lipids,* vol. 216, pp. 65-72, 2018.

[9] W. A. Al-Haj, H. Nsairat, and M. El-Tanani, "Pimozide-loaded nanostructured lipid carriers: Repurposing strategy against lung cancer," (in eng), *Sci Prog,* vol. 107, no. 4, p. 368504241296304, Oct-Dec 2024, doi: 10.1177/00368504241296304.

[10] K. Šimková, B. Joost, and G. Imanidis, "Production of fast-dissolving low-density powders for improved lung deposition by spray drying of a nanosuspension," *European Journal of Pharmaceutics and Biopharmaceutics,* vol. 146, pp. 19-31, 2020.

[11] H. I. Pass, "Lung cancer surveillance: new technologies and novel strategies," *Annals of Surgical Oncology,* vol. 7, no. 3, p. 171, 2000.

[12] N. R. Labiris and M. B. Dolovich, "Pulmonary drug delivery. Part II: the role of inhalant delivery devices and drug formulations in therapeutic effectiveness of aerosolized medications," *British journal of clinical pharmacology,* vol. 56, no. 6, pp. 600-612, 2003.

[13] F. Iskandar, L. Gradon, and K. Okuyama, "Control of the morphology of nanostructured particles prepared by the spray drying of a nanoparticle sol," *Journal of Colloid and interface Science,* vol. 265, no. 2, pp. 296-303, 2003.

[14] S. Javed, B. Mangla, Y. Almoshari, M. H. Sultan, and W. Ahsan, "Nanostructured lipid carrier system: A compendium of their formulation development approaches, optimization strategies by quality by design, and recent applications in drug delivery," *Nanotechnology Reviews,* vol. 11, no. 1, pp. 1744-1777, 2022.

[15] A.-K. Tuderman, C. J. Strachan, and A. M. Juppo, "Isomalt and its diastereomer mixtures as stabilizing excipients with freeze-dried lactate dehydrogenase," *International Journal of Pharmaceutics,* vol. 538, no. 1-2, pp. 287-295, 2018.

[16] N. Aditya *et al.*, "Development and evaluation of lipid nanocarriers for quercetin delivery: A comparative study of solid lipid nanoparticles (SLN), nanostructured lipid carriers (NLC), and lipid nanoemulsions (LNE)," *LWT-Food Science and Technology,* vol. 59, no. 1, pp. 115-121, 2014.

[17] H. Nsairat *et al.*, "Lipid nanostructures for targeting brain cancer," *Heliyon,* vol. 7, no. 9, 2021.

[18] S. Das and A. Chaudhury, "Recent advances in lipid nanoparticle formulations with solid matrix for oral drug delivery," *Aaps Pharmscitech,* vol. 12, pp. 62-76, 2011.

[19] P. Mura, F. Maestrelli, M. D'Ambrosio, C. Luceri, and M. Cirri, "Evaluation and Comparison of Solid Lipid Nanoparticles (SLNs) and Nanostructured Lipid Carriers (NLCs) as Vectors to Develop Hydrochlorothiazide Effective and Safe Pediatric Oral Liquid Formulations," *Pharmaceutics*, vol. 13, no. 4*,* doi: 10.3390/pharmaceutics13040437.

[20] M. Elmowafy and M. M. Al-Sanea, "Nanostructured lipid carriers (NLCs) as drug delivery platform: Advances in formulation and delivery strategies," *Saudi Pharmaceutical Journal,* vol. 29, no. 9, pp. 999-1012, 2021/09/01/ 2021, doi: https://doi.org/10.1016/j.jsps.2021.07.015.

[21] S. Martins, I. Tho, D. Ferreira, E. Souto, and M. Brandl, "Physicochemical properties of lipid nanoparticles: effect of lipid and surfactant composition," *Drug development and industrial pharmacy,* vol. 37, no. 7, pp. 815-824, 2011.

[22] P. Tewa-Tagne, S. Briançon, and H. Fessi, "Preparation of redispersible dry nanocapsules by means of spray-drying: development and characterisation," *European Journal of Pharmaceutical Sciences,* vol. 30, no. 2, pp. 124-135, 2007.

[23] A. P. B. Ribeiro *et al.*, "Crystallization modifiers in lipid systems," *Journal of food science and technology,* vol. 52, pp. 3925-3946, 2015.

[24] A. Gordillo-Galeano and C. E. Mora-Huertas, "Solid lipid nanoparticles and nanostructured lipid carriers: A review emphasizing on particle structure and drug release," *European Journal of Pharmaceutics and Biopharmaceutics,* vol. 133, pp. 285-308, 2018.

[25] C. Yue-Xing *et al.*, "The effect of l-leucine on the stabilization and inhalability of spray-dried solid lipid nanoparticles for pulmonary drug delivery," *Journal of Drug Delivery Science and Technology,* vol. 46, pp. 474-481, 2018.

[26] C. Freitas and R. H. Müller, "Spray-drying of solid lipid nanoparticles (SLNTM)," *European Journal of Pharmaceutics and Biopharmaceutics,* vol. 46, no. 2, pp. 145-151, 1998.

[27] A. O. Al Khatib, M. El-Tanani, and H. Al-Obaidi, "Inhaled Medicines for Targeting Non-Small Cell Lung Cancer," (in eng), *Pharmaceutics,* vol. 15, no. 12, Dec 14 2023, doi: 10.3390/pharmaceutics15122777.

[28] S. F. Taveira, L. M. de Campos Araújo, D. C. de Santana, A. Nomizo, L. A. P. de Freitas, and R. F. Lopez, "Development of Cationic Solid Lipid Nanoparticles with Factorial Design-Based Studies for Topical Administration of Doxorubicin," 2012.

[29] S. A. Swidan, H. M. Ghonaim, A. M. Samy, and M. M. Ghorab, "Efficacy and in vitro cytotoxicity of nanostructured lipid carriers for paclitaxel delivery," *Journal of Applied Pharmaceutical Science,* vol. 6, no. 9, pp. 018-026, 2016.

[30] I. V. Zelepukin *et al.*, "Fast processes of nanoparticle blood clearance: Comprehensive study," *Journal of controlled release,* vol. 326, pp. 181-191, 2020.

[31] P. Kumar *et al.*, "Promises of a biocompatible nanocarrier in improved brain delivery of quercetin: Biochemical, pharmacokinetic and biodistribution evidences," *International journal of pharmaceutics,* vol. 515, no. 1-2, pp. 307-314, 2016.

[32] J. Pardeike, A. Hommoss, and R. H. Müller, "Lipid nanoparticles (SLN, NLC) in cosmetic and pharmaceutical dermal products," *International journal of pharmaceutics,* vol. 366, no. 1-2, pp. 170-184, 2009.

[33] K. Westesen, H. Bunjes, and M. Koch, "Physicochemical characterization of lipid nanoparticles and evaluation of their drug loading capacity and sustained release potential," *Journal of controlled release,* vol. 48, no. 2-3, pp. 223-236, 1997.

[34] T. Delmas *et al.*, "How to prepare and stabilize very small nanoemulsions," *Langmuir,* vol. 27, no. 5, pp. 1683-1692, 2011.

[35] Y.-C. Kuo and I.-C. Chen, "Evaluation of surface charge density and surface potential by electrophoretic mobility for solid lipid nanoparticles and human brain− microvascular endothelial cells," *The Journal of Physical Chemistry B,* vol. 111, no. 38, pp. 11228-11236, 2007.

[36] H. Bera *et al.*, "Novel pimozide-β-cyclodextrin-polyvinylpyrrolidone inclusion complexes for Tourette syndrome treatment," *Journal of Molecular Liquids,* vol. 215, pp. 135-143, 2016/03/01/ 2016, doi: https://doi.org/10.1016/j.molliq.2015.12.054.

[37] P. Sawunyama, L. Jiang, A. Fujishima, and K. Hashimoto, "Photodecomposition of a Langmuir−Blodgett film of stearic acid on TiO2 film observed by in situ atomic force microscopy and FT-IR," *The Journal of Physical Chemistry B,* vol. 101, no. 51, pp. 11000-11003, 1997.

[38] J. Ibarra *et al.*, "Synthesis and characterization of magnetite/PLGA/chitosan nanoparticles," *Materials Research Express,* vol. 2, pp. 1-17, 09/11 2015, doi: 10.1088/2053-1591/2/9/095010.

[39] Z. Song *et al.*, "Improving Breviscapine Oral Bioavailability by Preparing Nanosuspensions, Liposomes and Phospholipid Complexes," *Pharmaceutics,* vol. 13, p. 132, 01/20 2021, doi: 10.3390/pharmaceutics13020132.

[40] A. Bhanderi, F. Bari, and H. Al-Obaidi, "Evaluation of the impact of surfactants on miscibility of griseofulvin in spray dried amorphous solid dispersions," *Journal of Drug Delivery Science and Technology,* vol. 64, p. 102606, 2021.

[41] W. Mehnert and K. Mäder, "Solid lipid nanoparticles: Production, characterization and applications," *Advanced Drug Delivery Reviews,* vol. 64, pp. 83-101, 2012/12/01/ 2012, doi: https://doi.org/10.1016/j.addr.2012.09.021.

[42] R. Shah *et al.*, "Production techniques," *Lipid Nanoparticles: Production, Characterization and Stability,* pp. 23-43, 2015.

[43] V. Paramita, K. Iida, H. Yoshii, and T. Furuta, "Effect of additives on the morphology of spray-dried powder," *Drying Technology,* vol. 28, no. 3, pp. 323-329, 2010.

[44] R. V. Tonon, C. R. Grosso, and M. D. Hubinger, "Influence of emulsion composition and inlet air temperature on the microencapsulation of flaxseed oil by spray drying," *Food Research International,* vol. 44, no. 1, pp. 282-289, 2011.

[45] S. Aziz, "Trehalose physicochemical characteristics as a potential dry powder inhalation carrier for optimized aerosol generation," Christian-Albrechts Universität Kiel, 2015.

[46] A. Baldelli and R. Vehring, "Analysis of cohesion forces between monodisperse microparticles with rough surfaces," *Colloids and Surfaces A: Physicochemical and Engineering Aspects,* vol. 506, pp. 179-189, 2016.

[47] E. D. Wiklund *et al.*, "Cytotoxic effects of antipsychotic drugs implicate cholesterol homeostasis as a novel chemotherapeutic target," *International journal of cancer,* vol. 126, no. 1, pp. 28-40, 2010.

[48] E.-H. Dakir *et al.*, "The anti-psychotic drug pimozide is a novel chemotherapeutic for breast cancer," *Oncotarget,* vol. 9, no. 79, p. 34889, 2018.

[49] A. M. Faheem, A. A. Elkordy, and N. Uddin, "Fabrication and physicochemical characterisation of novel pimozide loaded PLGA nanoparticles," *British Journal of Pharmacy,* vol. 4, no. 1, 2019.

[50] A. Ulldemolins Iglesias *et al.*, "Perspectives of nano-carrier drug delivery systems to overcome cancer drug resistance in the clinics," 2021.

[51] J. Lee, M.-K. Choi, and I.-S. Song, "Recent Advances in Doxorubicin Formulation to Enhance Pharmacokinetics and Tumor Targeting," *Pharmaceuticals,* vol. 16, no. 6, p. 802, 2023.

[52] A. Khan, S. Khan, M. A. Khan, Z. Qamar, and M. Waqas, "The uptake and bioaccumulation of heavy metals by food plants, their effects on plants nutrients, and associated health risk: a review," *Environmental science and pollution research,* vol. 22, pp. 13772-13799, 2015.

[53] A. Khosa, S. Reddi, and R. N. Saha, "Nanostructured lipid carriers for site-specific drug delivery," *Biomedicine & Pharmacotherapy,* vol. 103, pp. 598-613, 2018.

[54] A. M. Price-Whelan *et al.*, "The Astropy Project: sustaining and growing a community-oriented open-source project and the latest major release (v5. 0) of the core package," *The Astrophysical Journal,* vol. 935, no. 2, p. 167, 2022.

[55] I. M. Abdulbaqi *et al.*, "Pulmonary delivery of anticancer drugs via lipid-based nanocarriers for the treatment of lung cancer: An update," *Pharmaceuticals,* vol. 14, no. 8, p. 725, 2021.

Declaration of interests

☒ The authors declare that they have no known competing financial interests or personal relationships that could have appeared to influence the work reported in this paper.

☐ The authors declare the following financial interests/personal relationships which may be considered as potential competing interests: